MASSACHUSETTS INSTITUTE OF TECHNOLOGY

LINCOLN LABORATORY

MILLSTONE HILL THOMSON SCATTER RESULTS FOR 1964

J. V. EVANS

Group 31

TECHNICAL REPORT 430

15 NOVEMBER 1967

LEXINGTON MASSACHUSETTS

ABSTRACT

Thomson scatter (incoherent backscatter) observations of the ionosphere were made at Millstone Hill at a wavelength of 68 cm during 1964, for 30-hour periods every two weeks. These data have been employed to derive the mean hourly F-region (200 to 700 km) electron density profile and electron and ion temperature curves in each month. The results are presented in this report, together with the derived seasonal variation of electron density (at 0600, 1200, 1800 and 2400 hours local time) and the average daytime (0900 to 1500) and nighttime (2100 to 0300) electron and ion temperature behavior.

Separate measurements with a 23-cm radar permitted the temperature results reported to be extended to lower altitudes (~130 km) and, in addition, provided information concerning the ionic constituents between 130 and 230 km.

Although 1964 was at sunspot minimum, the seasonal variation in f_0F2 was quite evident. It is shown that this feature is strictly associated with the peak of the layer and that densities above 400-km altitude are highest at the equinoxes. No seasonal variations of temperature are found which might be large enough to account for the phenomenon. At night the peak densities are highest in summer, and the temperatures at all altitudes highest in winter. This last effect is believed largely due to heat conducted from the protonosphere, which in winter continues to be heated by photoelectron escape from the conjugate ionosphere which remains sunlit throughout the night.

Accepted for the Air Force
Franklin C. Hudson
Chief, Lincoln Laboratory Office

CONTENTS

MILLSTONE HILL THOMSON SCATTER RESULTS FOR 1964

I. INTRODUCTION

A Thomson scatter (incoherent backscatter) radar has been employed at Millstone Hill, Westford, Massachusetts (42.6°N, 71.5°W) in routine measurements of F-region electron densities, electron and ion temperatures. Previous reports[1,2] have outlined the procedures by which these data are gathered and reduced, and the results of observations for the year 1963 were presented in Ref. 2. Here we present results for the year 1964, which happened to be at the minimum in the sunspot cycle.

Based upon the diurnal variation of temperature observed in 1963, we have attempted to explain two anomalous features in the behavior of f_oF2 at Millstone Hill: the summer and equinox evening increase and early morning (predawn) winter increase.[3,4] It is of interest, therefore, to see to what extent the 1964 results yield diurnal variations that are the same as those observed in 1963. For the most part, agreement between the two sets of results is remarkably good, and this lends considerable confidence to the results and to morphological descriptions given previously.[2-4] However, these explanations have been questioned by recent theoretical study which is discussed. New results are presented which point to the existence of F-region temperature rises associated with the arrival of fast photoelectrons from the conjugate ionosphere.

Beginning in 1964, we employed a second radar system operating at 23-cm wavelength to explore regions below 200-km altitude. Because the 23-cm radar employs a fully steerable antenna system, it is possible to place the ionospheric echoes at a range greater than the ground-clutter interference by directing the beam obliquely. The two radar systems cannot be operated simultaneously because a number of components (e.g., the transmitter power supply and water cooling equipment) are shared. However, by comparing the results obtained with the two systems at different times, it has been possible to construct curves of ion and electron temperatures over the height interval from 130 to 800 km. The 23-cm radar observations also yield the relative abundance of the heavy and light ions as a function of altitude, i.e., the percentage composition of O^+ ions and the sum of O_2^+ and NO^+ ions. This report presents the results obtained with the 23-cm radar in 1964. In the sections that follow, we begin by presenting the 68-cm radar results. Section II presents the observing procedure, and in Secs. III and IV we briefly review the method of reduction and the accuracy of the results. In Secs. V and VI the diurnal and seasonal variations of the observed parameters are presented and discussed. Section VII reviews observations in which predawn heating of the F-region due to photoelectrons arriving from the conjugate ionosphere was detected. Section VIII discusses the 68-cm results. Sections IX through XII present the 23-cm radar measurements in this same order, namely,

TABLE I

INCOHERENT BACKSCATTER OBSERVATIONS – 1964

Begin (EST)			End (EST)			Mean K_p
3 January	D	0900	4 January		1530	4_o
10 January	D	0900	11 January		1600	2+
17 January		1000	18 January		1600	2_o
31 January	D	1030	1 February		1600	3+
14 February		1030	15 February	q	1530	2_o
28 February		1500	29 February		1500	2+
13 March		0930	14 March		1600	2_o
27 March	q	0900	28 March	Q	1600	0+
10 April	q	0900	11 April		1600	2–
24 April	Q	0930	25 April		1600	2–
8 May	Q	0930	9 May	Q	1700	0+
22 May	q	1130	23 May		1500	1–
14 June		0800	15 June		1500	2–
27 June		0030	27 June		1500	1_o
10 July		0800	11 July		1500	2–
24 July	Q	1000	25 July		1530	1+
7 August		0830	8 August	q	1600	2–
21 August	q	1100	22 August		1530	2–
4 September		0800	5 September		1430	2_o
18 September	q	0800	19 September	Q	1530	1_o
2 October	q	0800	3 October		1500	1+
16 October	q	0800	17 October		1500	1+
30 October	Q	1100	30 October	Q	1630	1–
6 November	q	0900	7 November	Q	1600	1–
13 November	q	0900	14 November	Q	1500	0+
27 November	q	0900	27 November	q	1500	0+
3 December		0900	4 December	q	1600	1_o
17 December		0900	18 December		1530	2_o
29 December		0900	30 December		1600	1_o

observations, reduction, results and discussion. Section XIII provides a summary of the work accomplished with both radar systems.

II. 68-CM OBSERVING PROCEDURE

In 1963 the complete height range over which density and temperature measurements could be made (about 200 to 800 km) was examined once every 90 minutes, approximately. Observations were usually conducted for periods of 30 hours at a time at weekly intervals. During 1964 the interval between observing periods was increased to two weeks, but the time required to obtain complete density and temperature profiles was reduced to one hour. Thus the number of profiles obtained were only about 25 percent less than in 1963. This reduction in the amount of time to produce the profiles was accomplished by recording some of the signals for later non-real-time processing. Table I lists the periods during which the data were gathered, and indicates the mean value of the geomagnetic index K_p during these periods. It can be seen that apart from January, the days on which the equipment was operated were magnetically quiet.

Several changes were made to the equipment in order to increase its reliability and ease of operation, but these did not appreciably alter the sensitivity of the apparatus.[1]

III. 68-CM DATA REDUCTION

Prior to 1964 the electron and ion temperatures obtained from the radar signal spectra at Millstone Hill tended to overestimate T_i. The error (of the order of 10 percent) arose from the neglect in the computation of expected spectral shapes (Ref. 1) of the distortion introduced in the receiver by gating from the time base a portion equal in length to the transmitted pulse. That is, the frequency smearing introduced by transmitting a pulse was allowed for, but the additional broadening arising from gating the receiver was not. Thus, an entirely new set of theoretical spectra have been computed by using the proper weight function which allows for these instrumental effects (F. Perkins and T. Hagfors, private communication). The power in the i^{th} filter is

$$P_i(f)_{obs} = \int_{-\infty}^{+\infty} \langle |S(f)|^2 \rangle_{avg} \, F_i(f) \, df \tag{1}$$

where $\langle |S(f)|^2 \rangle_{avg}$ is the power spectrum at the output of the receiver, $F_i(f)$ is the power of i^{th} analyzer filter and f is frequency shift measured with respect to the translated radar frequency. The power spectrum $\langle |S(f)|^2 \rangle_{avg}$ presented to the spectrum analyzer filter bank is

$$\langle |S(f)|^2 \rangle_{avg} = \int_{-\infty}^{+\infty} d\nu \langle |H(\nu t_o)|^2 \rangle_{avg} \cdot \frac{4\tau}{[2\pi(f-\nu)]^2} \left[1 - \frac{\sin 2\pi(f-\nu)\tau}{2\pi(f-\nu)\tau}\right] \tag{2}$$

where $\langle |H(\nu t_o)|^2 \rangle_{avg}$ is the spectral broadening (of a CW signal) introduced by the ionosphere (as a function of frequency ν) corresponding to a delay t_o and τ is the pulse length employed. The equations for $\langle |H(\nu t_o)|^2 \rangle_{avg}$ have been given by a number of authors, e.g., Fejer.[5]

Besides being a function of electron-to-ion temperature ratio T_e/T_i, ion temperature T_i and ion composition, the spectral shape depends upon the electron density N. It was shown earlier that this latter dependence could be handled by obtaining from the experimental results an approximate electron density profile from which the density N could be estimated. The values of T_e/T_i and T_i were then established by comparison of the observed signal spectra with one

computed for the same density. In practice, only a limited number of cases for different densities were worked out, namely, corresponding to plasma frequencies f_N = 1.0, 1.5, 2.0, 2.5, 5.0 and 10 MHz ($N = 1.24 \times 10^4 f_N^2$, N in electrons/cm^3, f_N in MHz). For wavelength in use at Millstone Hill (λ = 68 cm) it transpires that the signal spectral shape ceases to change when $f_N \geq 5$ MHz.

In the new computations, theoretical spectra have been computed only for the case f_N = 10 MHz. Following the suggestion of Moorcroft,[6] these are employed to derive values of T_e/T_i and T_i which will be correct if $f_N \geq 5$ MHz. If the plasma frequency is less than ~5 MHz, only T_i will be correct and the derived electron-to-ion temperature ratio $(T_e/T_i)'$ will be related to the true ratio (T_e/T_i) in

$$\left(\frac{T_e}{T_i}\right)' = \frac{\alpha^2}{1+\alpha^2}\left(\frac{T_e}{T_i}\right) \tag{3}$$

where $\alpha = \lambda/4\pi D$ and $D = \sqrt{(kT_e/4\pi Ne^2)}$ is the Debye length. For Millstone, $\alpha = 0.785\sqrt{(N/T_e)}$ when the density N is expressed in electrons/cm^3. It follows that it is a relatively simple matter to produce a set of curves from which T_e can be read off, given N and T_e'.

The procedure for analyzing the data is now as follows. The signal spectra are scaled to yield two quantities: f the width in kilohertz between the center and a value of half-peak intensity, and x the ratio of the peak intensity (in the wings) to that at the center frequency. These values are inserted on a graph appropriate to the pulse length employed (τ = 0.5 or 1.0 msec) to yield values of T_i and T_e'/T_i. The electron density profile is then obtained in the manner outlined previously except that the factor employed to correct for the effect of the temperature inequality ($T_e > T_i$) becomes[6,7]

$$N(\text{true}) = \frac{2}{1 + T_e'/T_i}\, N(\text{obs}) \tag{4}$$

which is a closer approximation than used hitherto,[1,2] namely

$$N(\text{true}) = \frac{2}{1 + T_e/T_i}\, N(\text{obs}) \tag{5}$$

Given the true density N at the height where the temperature measurement was made, the true value of T_e is obtained by interpolation from a plot of T_e vs T_e' and N [Eq. (3)] as outlined above. As in the past, the method by which the electron density profiles are constructed depends upon the radar data only for the height and shape of the profile. The absolute density at all heights is established by normalizing the peak density to the value of $N_{max}F2$ observed with an ionosonde.

From all these data, mean hourly electron density and temperature profiles are constructed for each month. In the case of the density N, this requires that the relative density N/N_{max} must be determined at fixed intervals, e.g., ±25, ±50, ±75, ±100... km, measured with respect to the peak. A mean of these is obtained which yields a mean profile with the correct shape. This is then assigned the mean value of h_{max} and N_{max}. For the temperature profiles the mean electron and ion temperatures at the heights sampled are computed, and the best smooth curve is drawn through these points. These vertical profiles are then used to plot contours of constant density N (expressed as a plasma frequency f_N) and temperature as a function of height and time over the day. This type of presentation provides the greatest amount of reduction in the number of data points obtained.

In addition to the analysis outlined above, mean daytime and nighttime temperature profiles for each month are constructed by averaging all the data obtained during the periods from 0900 to 1500 EST and from 2100 to 0300 EST, respectively. These curves are then used to obtain plots of isothermal contours vs height and month for the entire year. These plots may be employed to infer daytime and nighttime seasonal variations.

IV. ACCURACY OF 68-CM RESULTS

It is thought that sources of instrumental error,[1] which were bothersome during the first half of 1963, were eliminated by 1964.[2] Accordingly, the principal sources of systematic error are the assumptions made during the analysis. The first of these is that only O^+ ions are present at all heights. There is some evidence (Sec. XII-A) that at the lowest altitude observed, i.e., with the pulse center at 225 km, regions with an appreciable percentage of NO^+ or O_2^+ ions are included by the large vertical extent of the pulse (±35 km approximately). The error in the temperature measurements for 225-km altitude as a consequence of this effect appears to be −10 percent or less, and is significant chiefly in lowering the value of T_i obtained at this altitude by about 50°K.

At the highest altitudes (>600 km) there is the possibility that a small number of light ions are present. This would lead to an overestimate of T_i and a somewhat smaller overestimate of T'_e. The exact height of the transition region from O^+ ions to He^+ and H^+ ions is known to be lowest at sunspot minimum.[8,9] There is also evidence that it is higher during the day than at night and that it is higher at temperate latitudes than over the equator.[10] Unfortunately, no satellite-borne mass-spectrometer measurements for 1964 have been published, yet by various indirect methods the height of the transition altitude has been inferred for this period. Watt[11] has employed topside soundings obtained with the Alouette I sounder, together with certain assumptions concerning the behavior of the electron and ion temperatures with altitude, to infer the transition height. At the dip latitude of Millstone (73°), Watt[11] finds that the transition altitude (defined as the height of 50% O^+, 50% He^+ or H^+ ions) lies above the satellite (i.e., >1000 km) during the day and at ≥900 km during the night. The altitude of the transition lies sufficiently beneath the satellite that it can be located with reasonable certainty only over the range of dip latitudes 48° to 60°. Using the same satellite, Barrington, et al.,[12] were able to infer some information concerning the ion composition at 1000-km altitude by determining the cutoff frequency of a VLF emission together with the scale height of the F-region at the satellite. At a height of 1000 km above Millstone ($L = 3.5$), Barrington, et al., find less than 20% H^+ ions during 6-hour periods centered on 0600 and 1800 local mean time. The only recent rocket flights into the topside ionosphere from which ion composition could be determined indicated that He^+ never became the predominant ion.[9] Bauer has suggested that this is typical behavior at sunspot minimum,[9] in which case the estimates of Barrington, et al., concerning the H^+ abundance may be taken as close to the total abundance of light ions.

From the foregoing it would appear that the upper limit at which temperature determinations can be made with this apparatus (approximately 800 km by day and 600 km by night) lies at least one scale height (i.e., ~200 km) below the transition altitude at all times. We may expect, therefore, that the light ion abundance is of the order of 10 percent or less at the highest altitude that can be examined. Thus we believe that the error introduced by the neglect of the presence of light ions is substantially less than postulated earlier.[1]

V. DIURNAL VARIATIONS OBSERVED AT 68 CM

Figures 1 through 12 present the results for the months January through December. In each figure (a) contains the results for the electron density, (b) the electron temperature and (c) the ion temperature.

A. Electron Density

The behavior of the electron density [Figs. 1(a) through 12(a)] shows a striking degree of similarity from month to month. For example, h_{max} is always highest (~290 to 300 km) near midnight and falling between midnight and dawn. The value of h_{max} reaches a minimum about two hours after ground sunrise (Table II) and thereafter tends to rise, with the rate of increase being fastest after sunset.

TABLE II

SUNRISE AND SUNSET AT 100-KM ALTITUDE (χ = 98.5° at Ground Level) FOR MILLSTONE HILL AND ITS MAGNETICALLY CONJUGATE POINT

Date	Millstone Hill (42.6°N 71.5°W)		Conjugate Point (71.9°S 80.7°W)	
	Sunrise (EST)	Sunset (EST)	Sunrise (EST)	Sunset (EST)
1 January	0629	1709	↑	↑
15 January	0628	1722	Always sunlit	
1 February	0617	1742		
15 February	0602	1759	↓	↓
1 March	0541	1816	0220	2251
15 March	0518	1832	0405	2059
1 April	0448	1853	0531	1923
15 April	0423	1910	0632	1814
1 May	0356	1930	0737	1703
15 May	0337	1948	0831	1607
1 June	0320	2007	0928	1512
15 June	0315	2017	0958	1447
1 July	0320	2019	0958	1454
15 July	0330	2012	0928	1528
1 August	0350	1955	0832	1627
15 August	0407	1935	0735	1720
1 September	0428	1905	0619	1829
15 September	0444	1839	0508	1929
1 October	0501	1811	0334	2051
15 October	0516	1747	0134	2244
1 November	0536	1713	↑	↑
15 November	0552	1709	Always sunlit	
1 December	0619	1700		
15 December	0621	1700	↓	↓

The electron density increases throughout the morning at all altitudes and tends to reach a maximum around noon or shortly thereafter. If one allows for the fact that the layer is rising, it is clear that at fixed heights with respect to h_{max} the density tends to decrease in the afternoon at all altitudes until the evening increase occurs. This phenomenon has been the subject of a separate article[3] which suggested that the rapid fall of electron temperature during sunset gives rise to a collapse in the layer thickness and an increase in the density at the peak. In summer this is sufficiently pronounced for f_oF2 to reach its highest value at this time of day. Variability in the increase of f_oF2 from day to day could be related to the height to which h_{max} has risen during the course of the day. Thus, though the rapid fall in electron temperature was proposed as the prime physical agent, the forces that are responsible for driving the layer upward were thought to exert a modifying influence. The evening increase is evident in all months at heights well above h_{max} but can be recognized in f_oF2 only during equinox and summer. It was suggested[3] that this is because (a) in winter the fall in T_e is neither large nor rapid, (b) in winter the amount of ionization above h_{max} that can participate is less, and (c) the density at the peak is already high.

This explanation has been challenged by Thomas and Venables[13] who succeeded in solving the time-dependent continuity equation for the F-region when the electron and ion temperatures are allowed to vary independently. Their results show that, though the electron temperature decrease at sunset is capable of causing ionization to diffuse to lower altitudes, this in itself is not able to give rise to increases in electron density as large as observed. They suggest that the prime cause is the temperature dependence of the principal loss mechanism at F-region heights, namely

$$O^+ + N_2 \rightarrow NO^+ + N \qquad (6)$$

$$NO^+ + e \rightarrow N + O + h\nu \qquad (7)$$

If the N_2 molecules which take part [Eq. (6)] are vibrationally excited, the effective rate coefficient would be a function of vibrational temperature. Thus, if it is assumed that the vibrational temperature has a similar diurnal variation to the electron temperature, the rapid decrease in T_e at sunset would give rise to a marked change in the loss rate and could result in an accumulation of ionization near the peak.[13]

In summer the evening maximum in f_oF2 is larger than the noon maximum, but in equinox the midday maximum tends to be larger. In winter, as already noted, the evening increase is an observable effect only above about 300-km altitude, so that f_oF2 shows a single midday maximum.

In summer and equinox the densities decrease at all altitudes throughout the night. In winter this decrease is arrested near 2200 EST at heights below 450 km and a maximum occurs near 0400. Above 500 km the density appears to be decreasing throughout the night. It has been suggested that this redistribution of ionization in the F-region is caused by the cooling of the whole protonosphere.[4] It was supposed that such cooling would be most serious following sunset in the conjugate hemisphere, or in the absence of sunset when the sun's zenith angle becomes large. A closer examination of the zenith distance of the sun at the conjugate point shows that it is less than $\chi = 90°$ throughout the night. Further, there is no change in the angle β between the sun and the field which could cause a significant change in the pitch angle distribution and

hence the escape rate of photoelectrons.[14] The most plausible explanation at this time is to suppose that the reduced electron temperature that accompanies the density increase is responsible for reduced loss rates and consequently the density increase itself. The reason for a temperature decline must be sought in the behavior of the photoelectron escape flux at the conjugate point.

B. Electron Temperature

During equinoctial months (March, April, September and October) the electron temperature [Figs. 3(b), 4(b), 9(b), 10(b)] rises rapidly at sunrise, is roughly constant at all altitudes throughout the day and falls somewhat less rapidly at sunset. During the day there is a positive temperature gradient of about 2°/km at all altitudes. Similar electron temperature behavior is observed in summer months [Figs. 6(b)-8(b)] though there appears to be an early morning maximum at some altitudes. In winter months [Figs. 1(b), 2(b), 11(b), 12(b)] the temperature gradient above 300 km is higher than in summer (~3°/km), but the actual temperature near $h_{max}F2$ is lower. At night in all seasons the electron temperature exceeds the ion temperature. This is thought to be a consequence of heat supplied by the protonosphere[15] as argued previously;[2] however, it is probable that during the winter months when the conjugate hemisphere remains sunlit, photoelectrons traverse the protonosphere and contribute to the nocturnal heating of the local ionosphere (Sec. VII).

During the short summer night the electron temperature is roughly constant at a given altitude. In the equinoxes the temperature reaches a minimum a little before midnight [Figs. 4(b), 9(b)] and then increases again. In winter the same thing happens, except that the reversal from cooling to warming occurs only 2 hours after local sunset. This behavior is believed to be a consequence of the fact that the protonospheric heat flux is roughly constant throughout the night[16] and the heat loss (from electrons to ions) initially exceeds the input, but later as the density decreases this situation is reversed.

C. Ion Temperature

The diurnal variation of T_i above 300-km altitude tends to follow that of the electron temperature, thereby demonstrating the thermal coupling between the two. During the daytime the ion temperature remains fairly constant at all altitudes. In summer T_i declines throughout the night. In winter T_i shows little evidence of sunset and does not decrease appreciably till 0200 EST when the electron temperature is also found to be declining rapidly. In Ref. 4 we argued that this was a consequence of the increase in density [e.g., Figs. 1(a), 2(a)] which occurs at this time and causes a second reversal in the balance between heating and cooling. In the tentative explanation given above, cause and effect have been reversed.

In all seasons the daytime temperature gradient above 400 km is of the order of 4°/km, suggesting that the ion temperature is greater than that of the neutrals, and is converging on the electron temperature. Below 300 km the ions are probably in good thermal equilibrium with the neutrals, but the values shown in Figs. 1(c) – 12(c) (toward the bottoms of the figures) are probably too low (Sec. IV). During the night in equinox and in summer, the temperature gradient dT_i/dh appears somewhat lower than during the day (~1.5°/km).

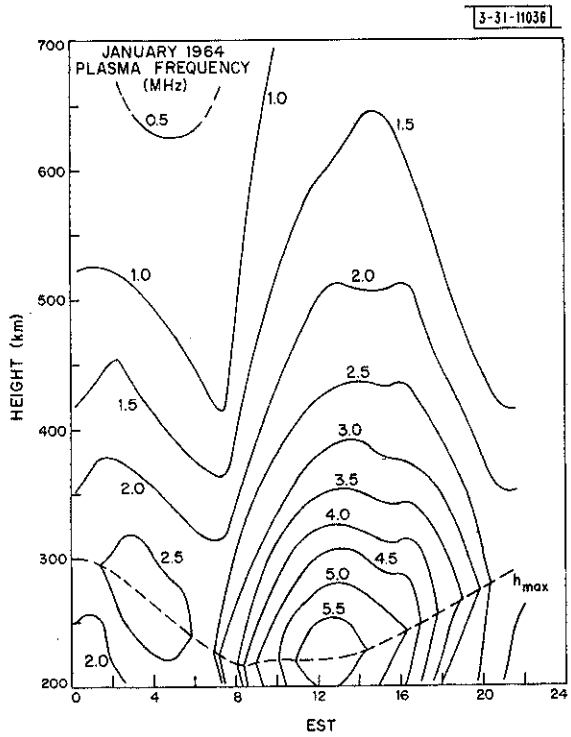

(a) Plasma frequency.

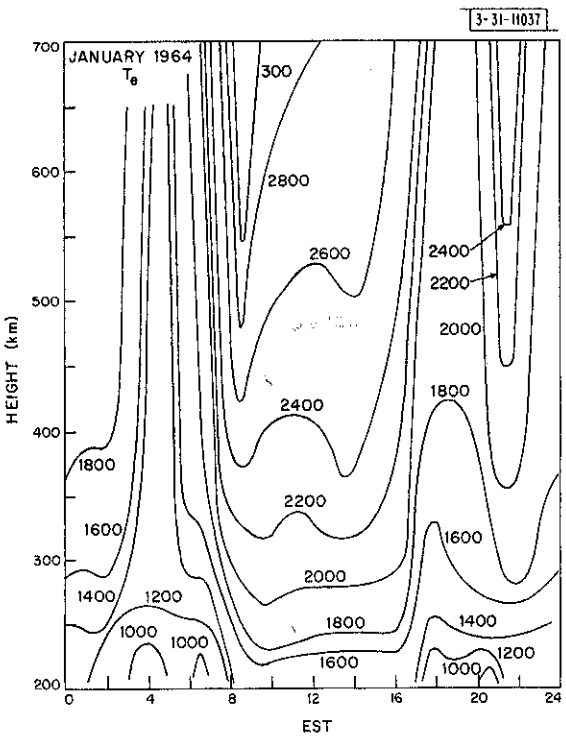

(b) Electron temperature.

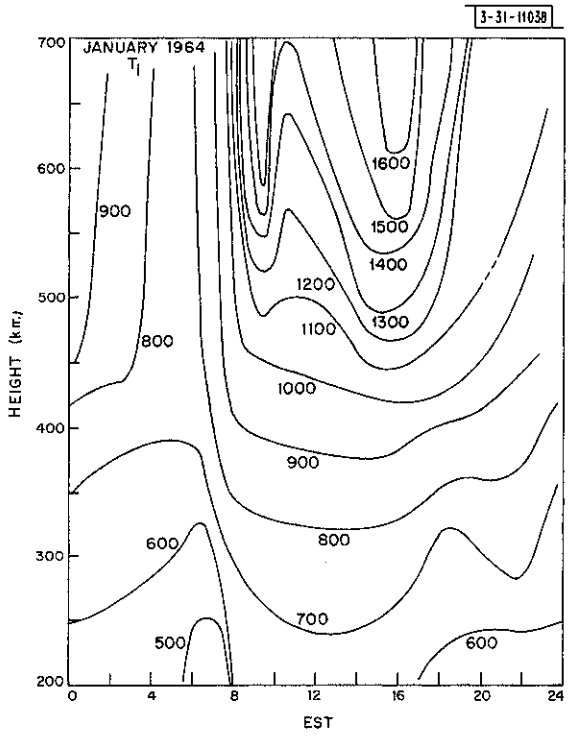

(c) Ion temperature.

Fig. 1. Mean monthly behavior for January 1964.

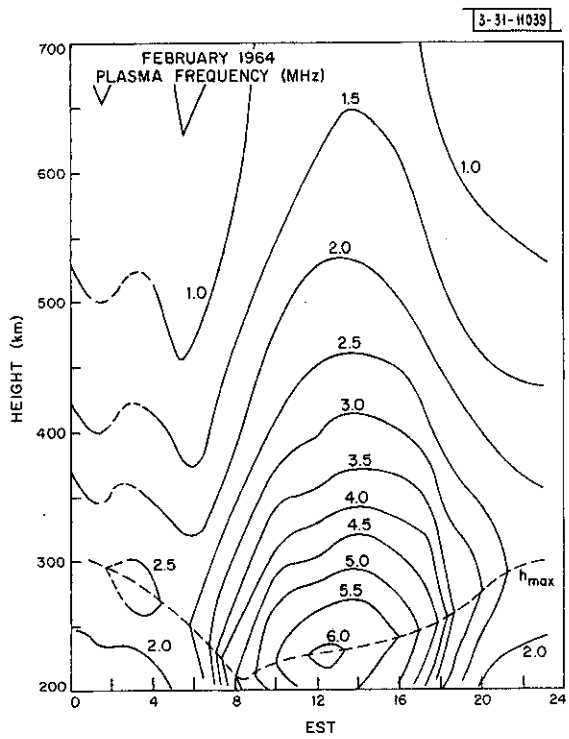

(a) Plasma frequency.

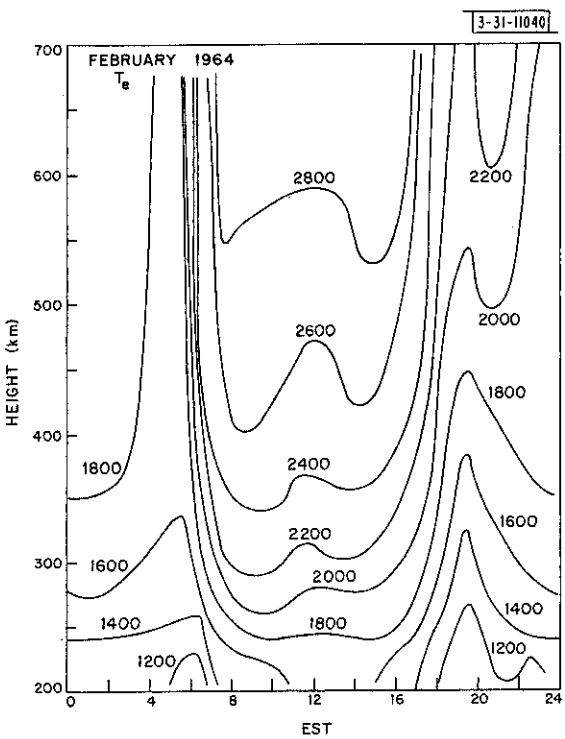

(b) Electron temperature.

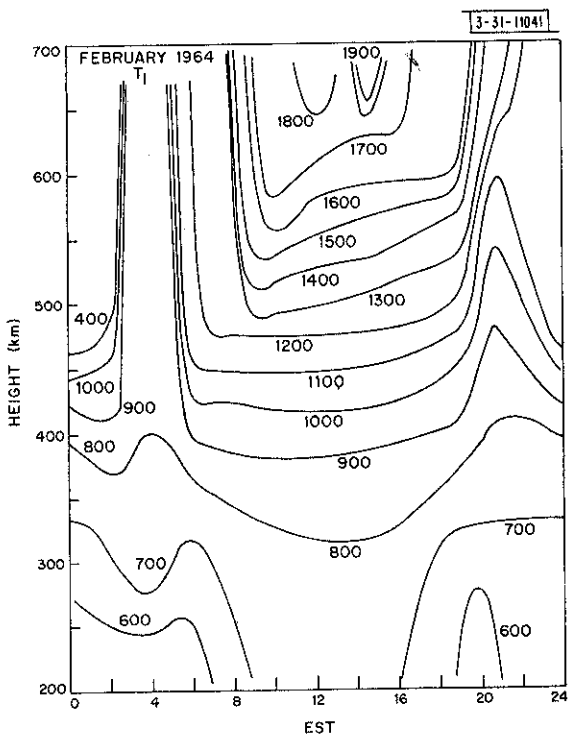

(c) Ion temperature.

Fig. 2. Mean monthly behavior for February 1964.

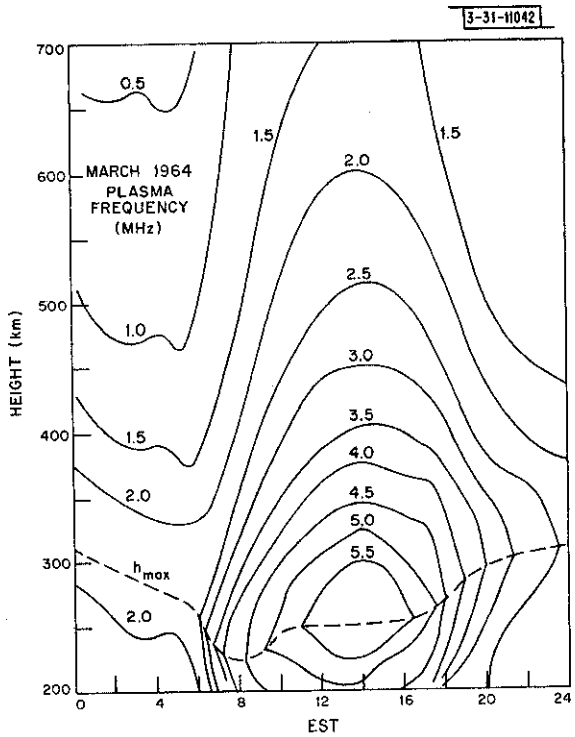

(a) Plasma frequency.

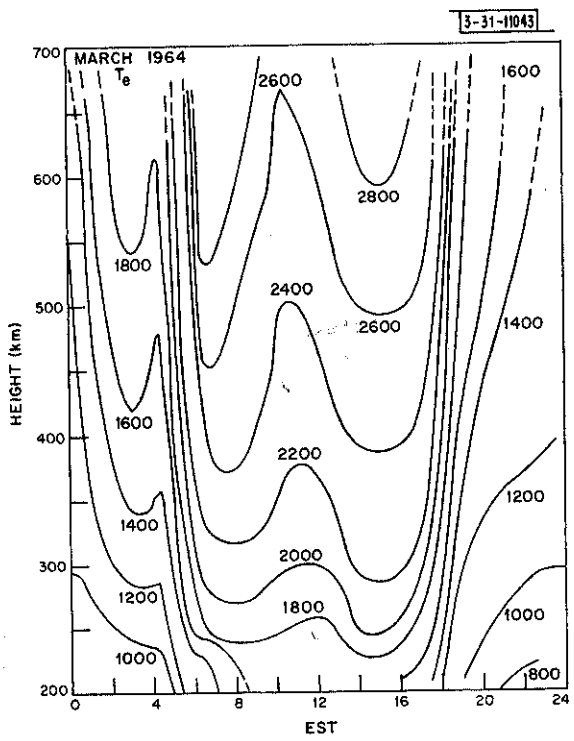

(b) Electron temperature.

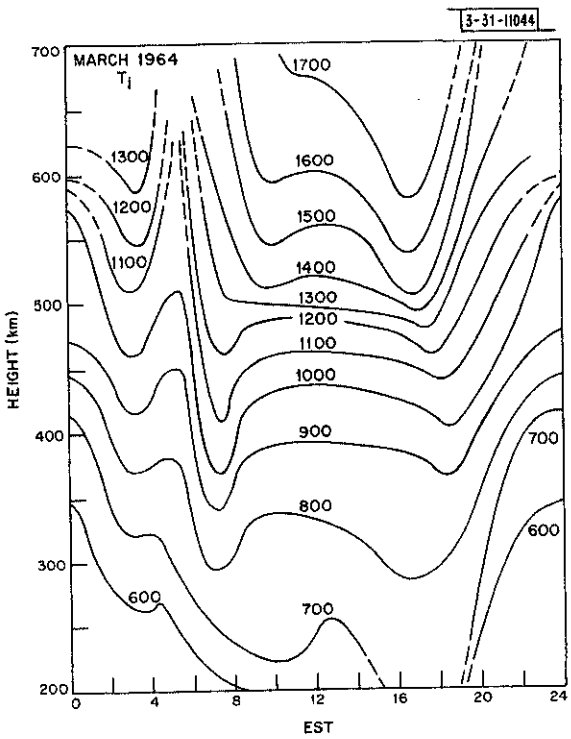

(c) Ion temperature.

Fig. 3. Mean monthly behavior for March 1964.

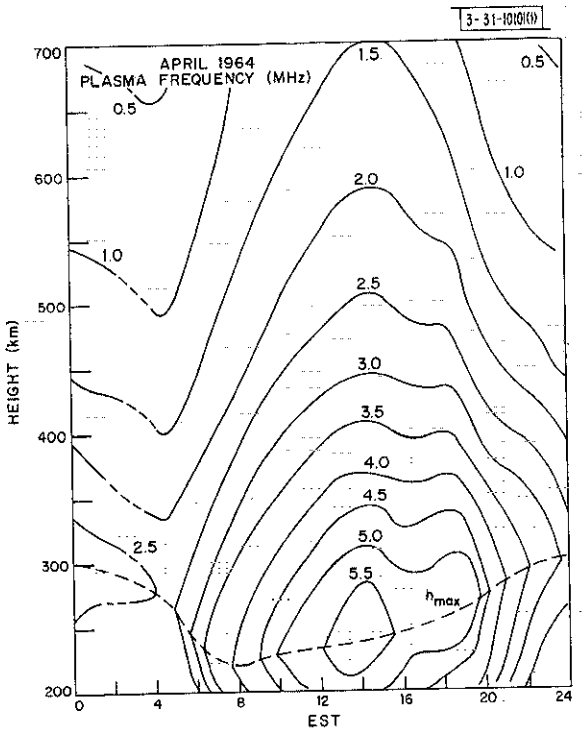

(a) Plasma frequency.

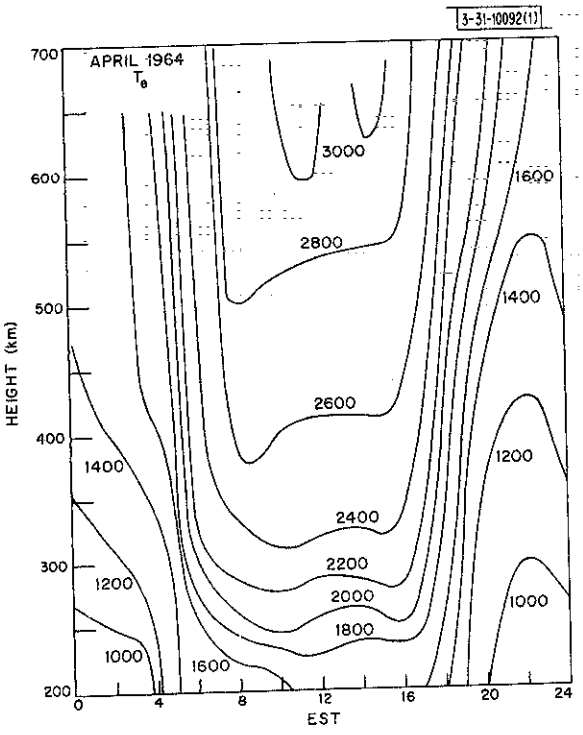

(b) Electron temperature.

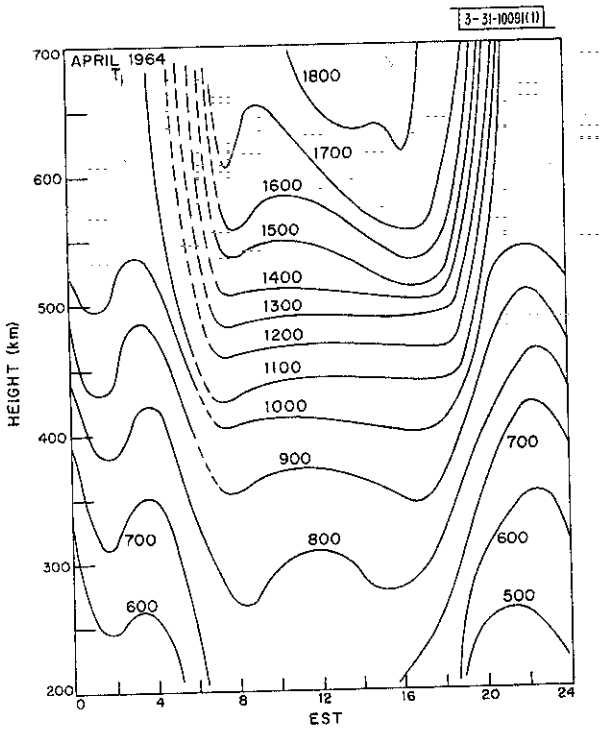

(c) Ion temperature.

Fig. 4. Mean monthly behavior for April 1964.

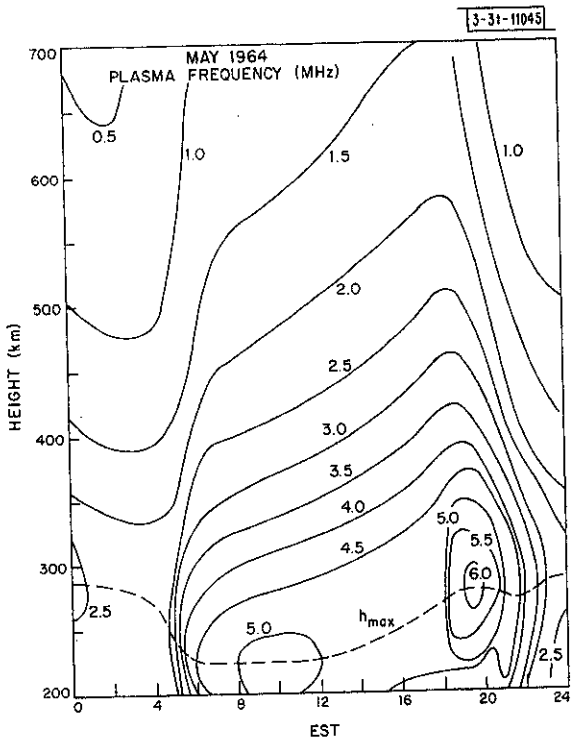

(a) Plasma frequency.

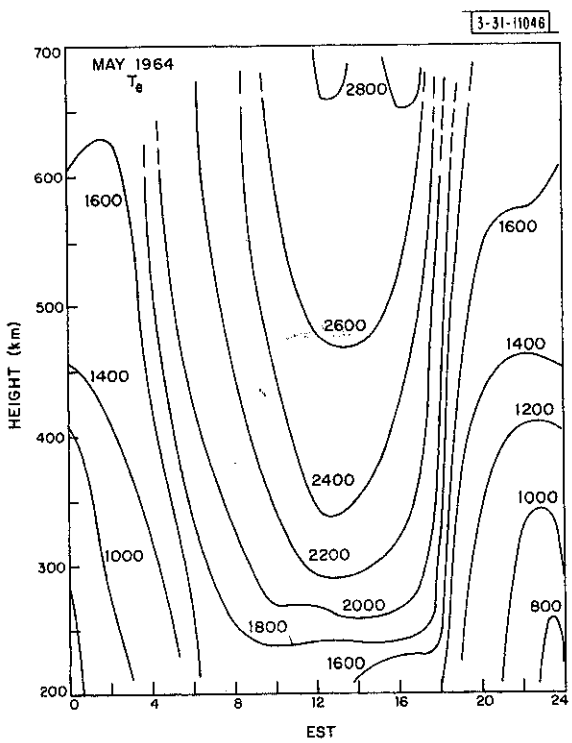

(b) Electron temperature.

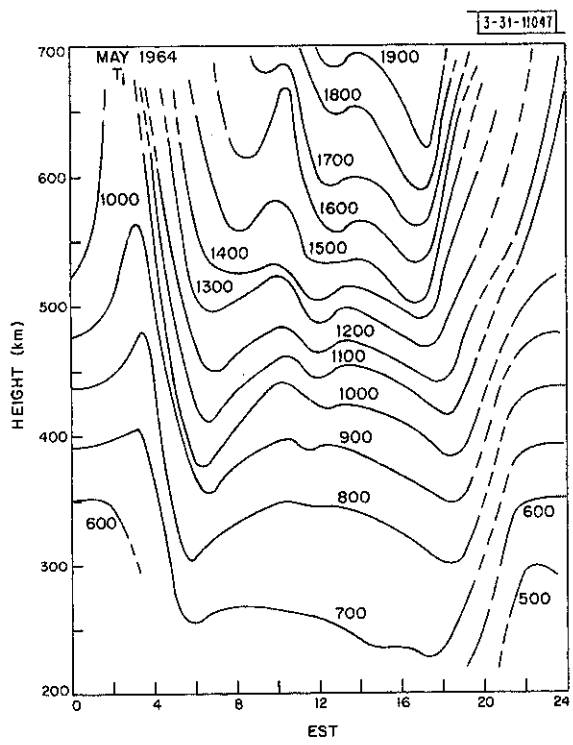

(c) Ion temperature.

Fig. 5. Mean monthly behavior for May 1964.

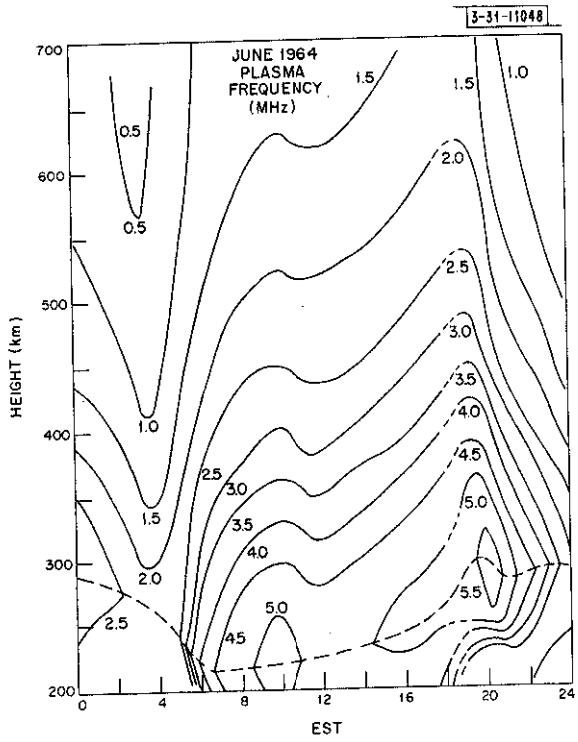

(a) Plasma frequency.

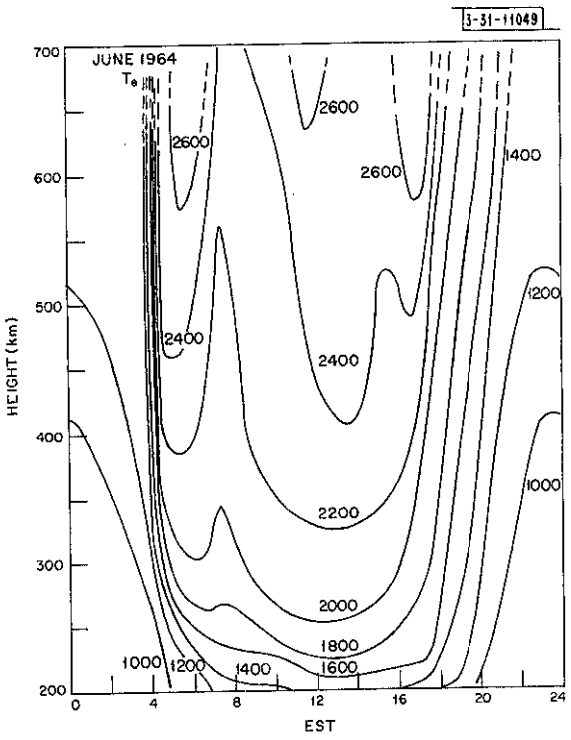

(b) Electron temperature.

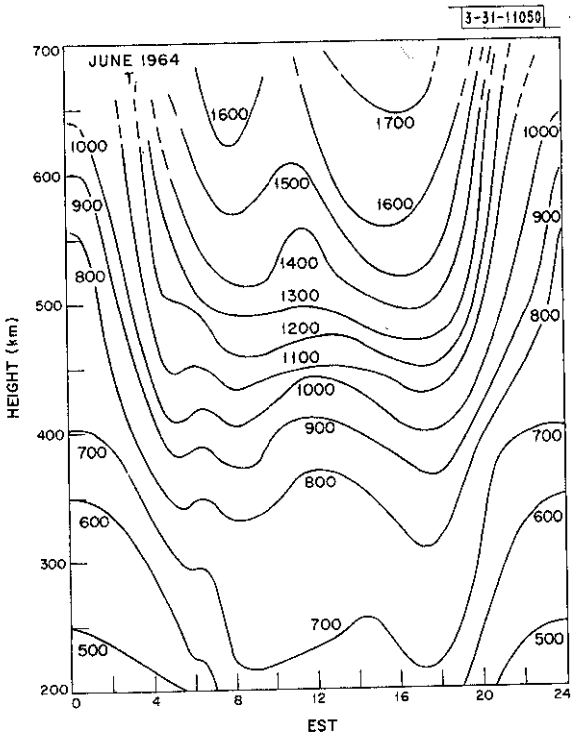

(c) Ion temperature.

Fig. 6. Mean monthly behavior for June 1964.

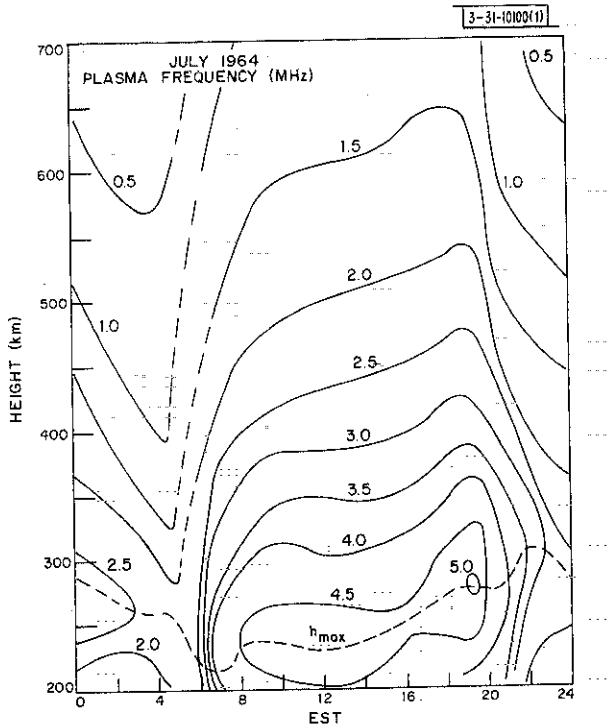

(a) Plasma frequency.

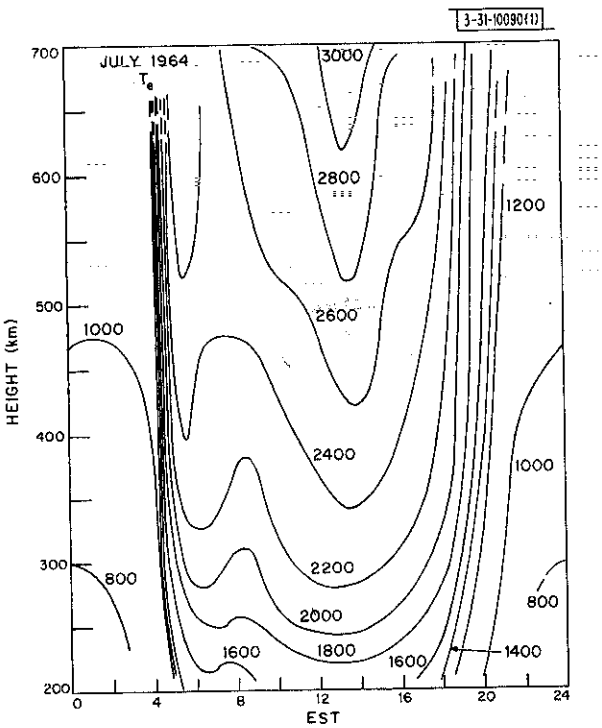

(b) Electron temperature.

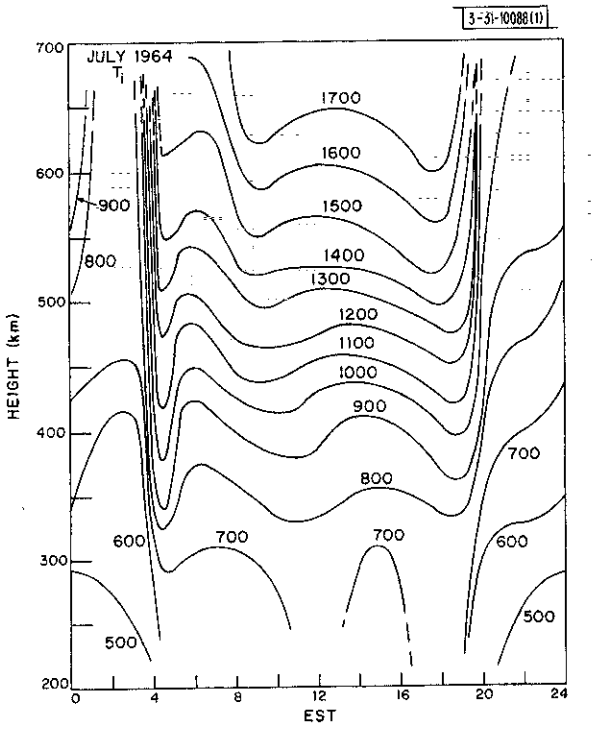

(c) Ion temperature.

Fig. 7. Mean monthly behavior for July 1964.

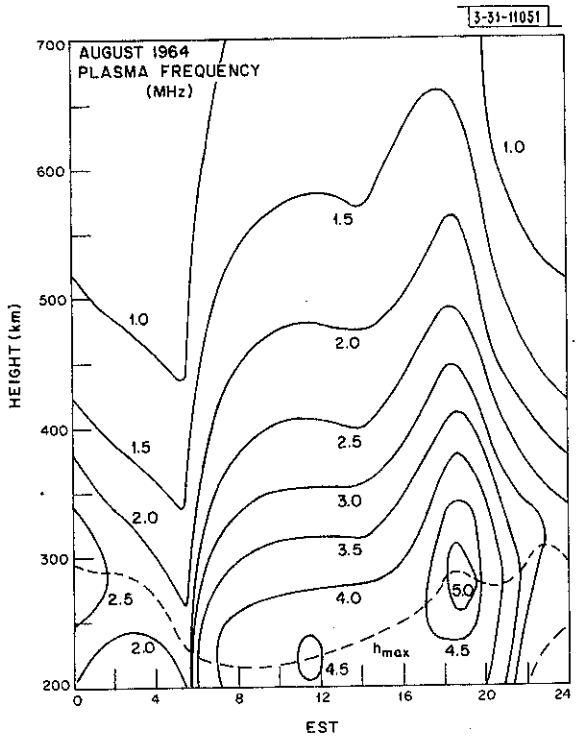

(a) Plasma frequency.

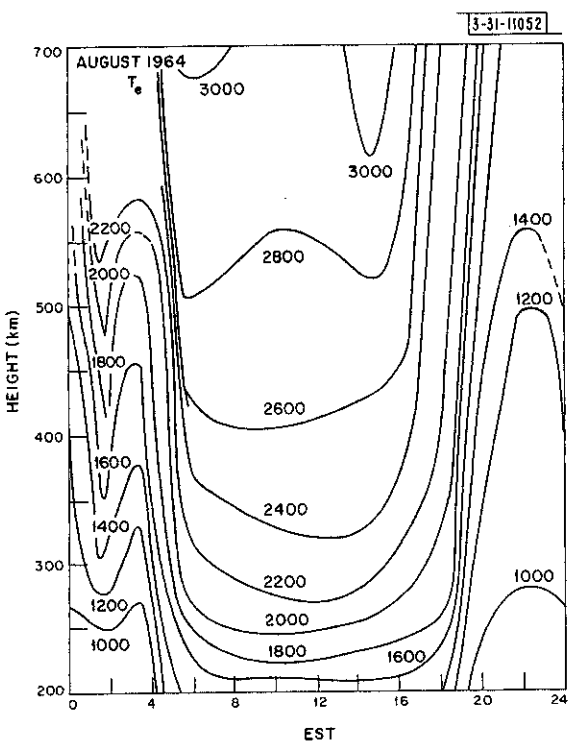

(b) Electron temperature.

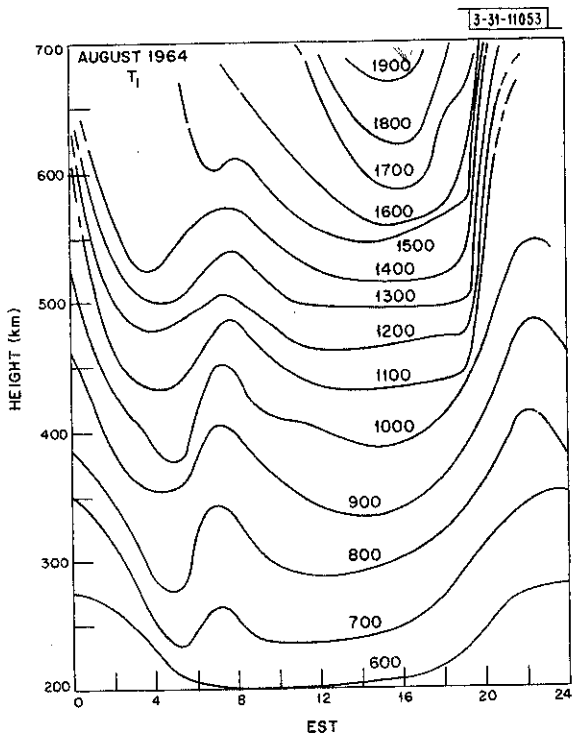

(c) Ion temperature.

Fig. 8. Mean monthly behavior for August 1964.

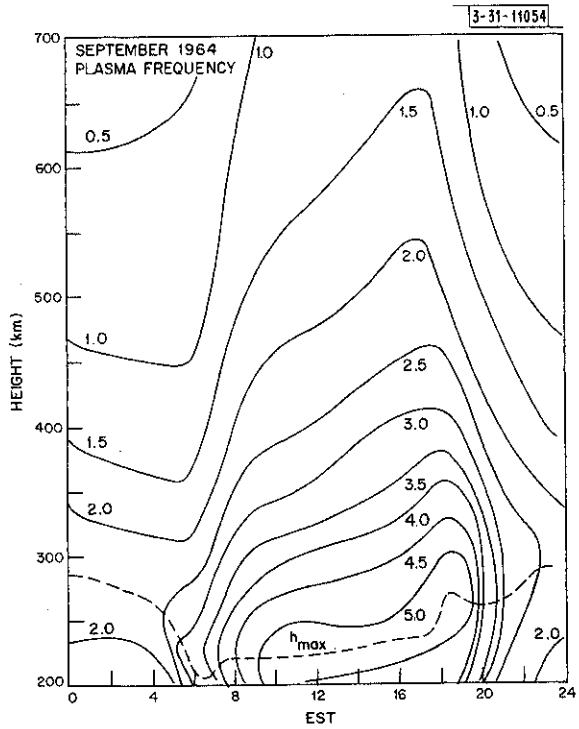

(a) Plasma frequency.

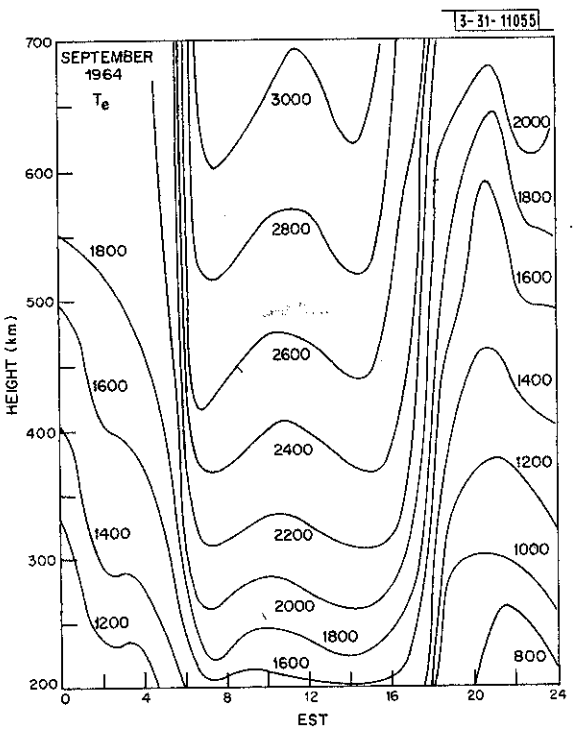

(b) Electron temperature.

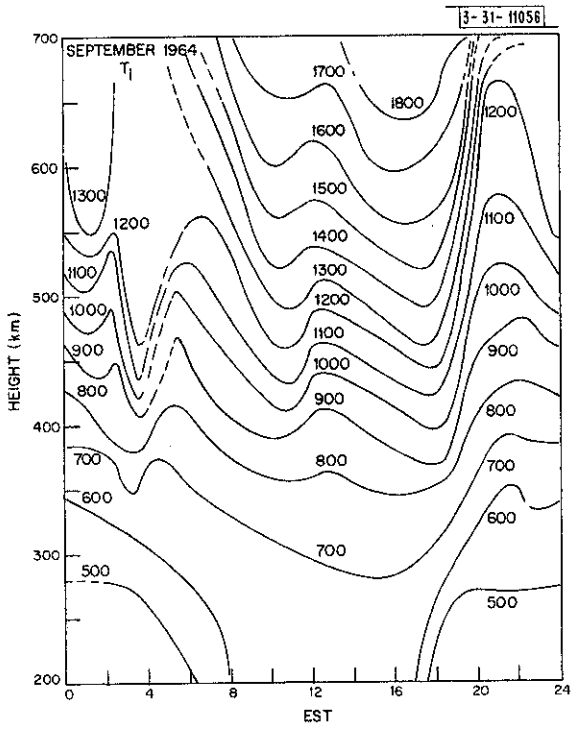

(c) Ion temperature.

Fig. 9. Mean monthly behavior for September 1964.

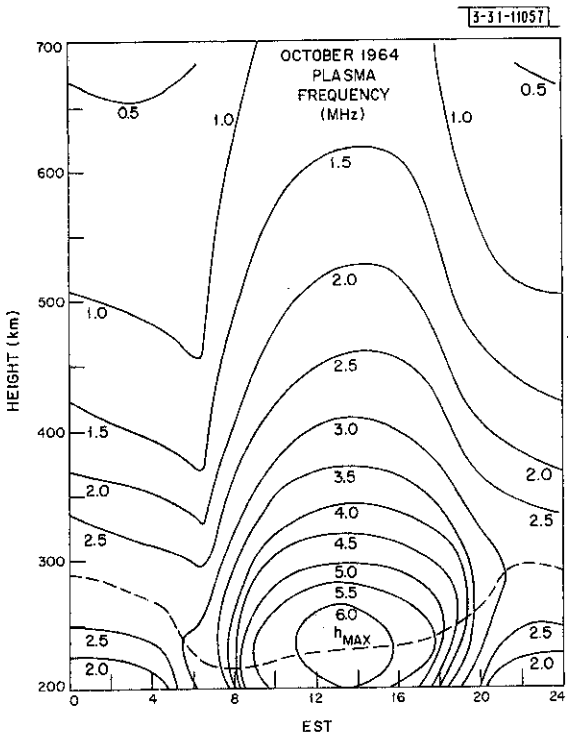

(a) Plasma frequency.

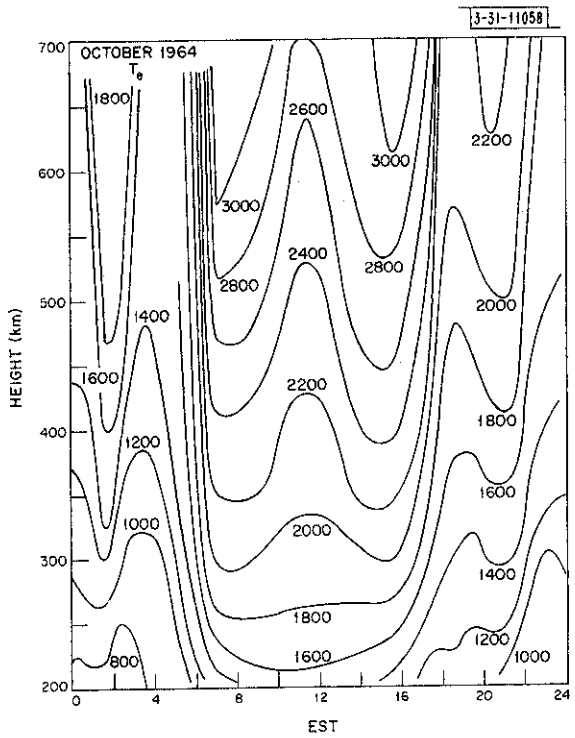

(b) Electron temperature.

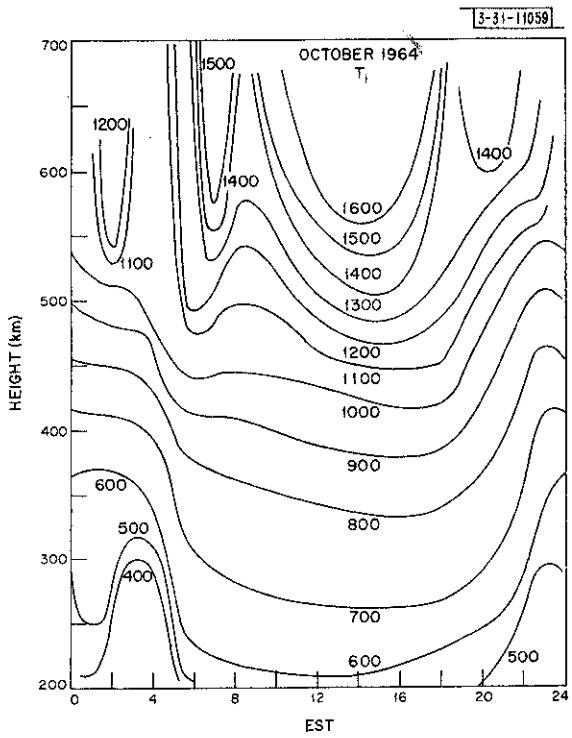

(c) Ion temperature.

Fig. 10. Mean monthly behavior for October 1964.

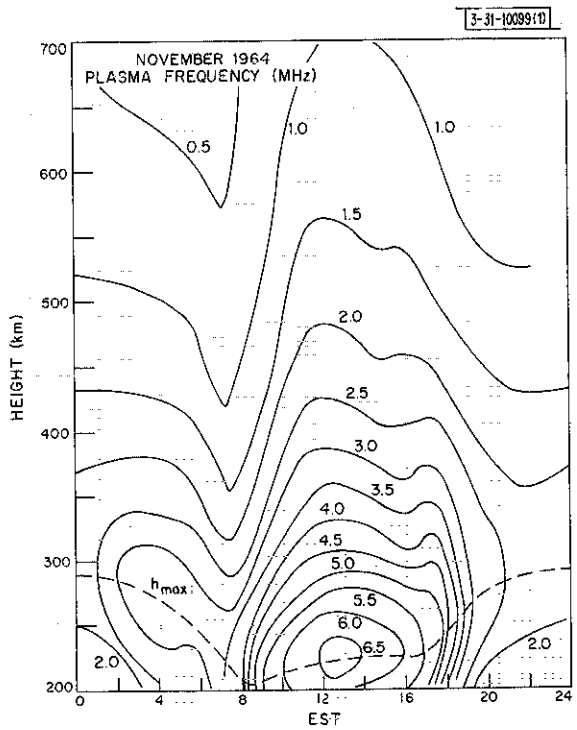

(a) Plasma frequency.

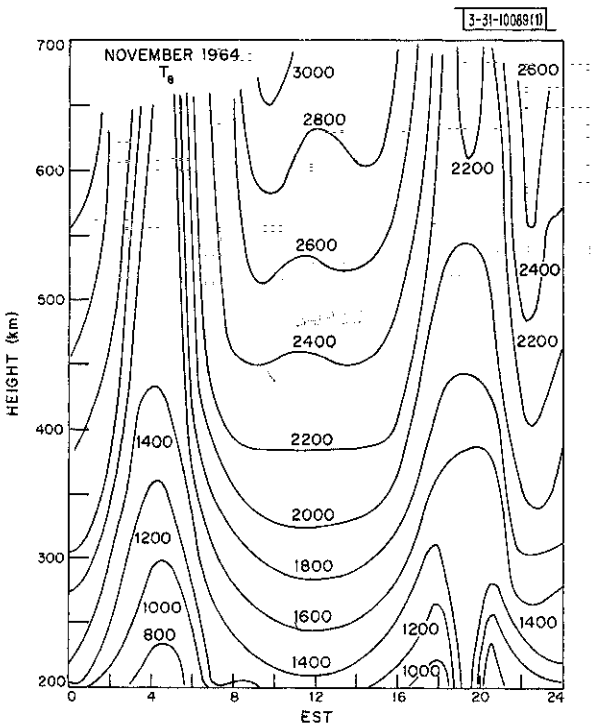

(b) Electron temperature.

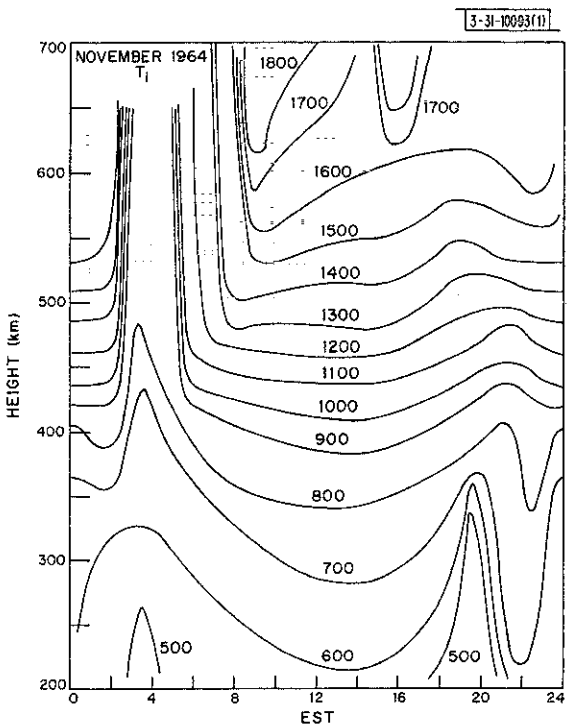

(c) Ion temperature.

Fig. 11. Mean monthly behavior for November 1964.

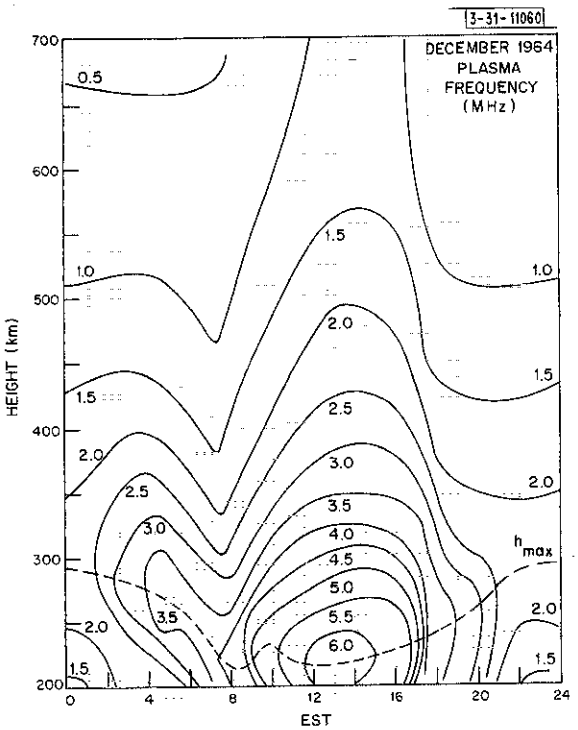

(a) Plasma frequency.

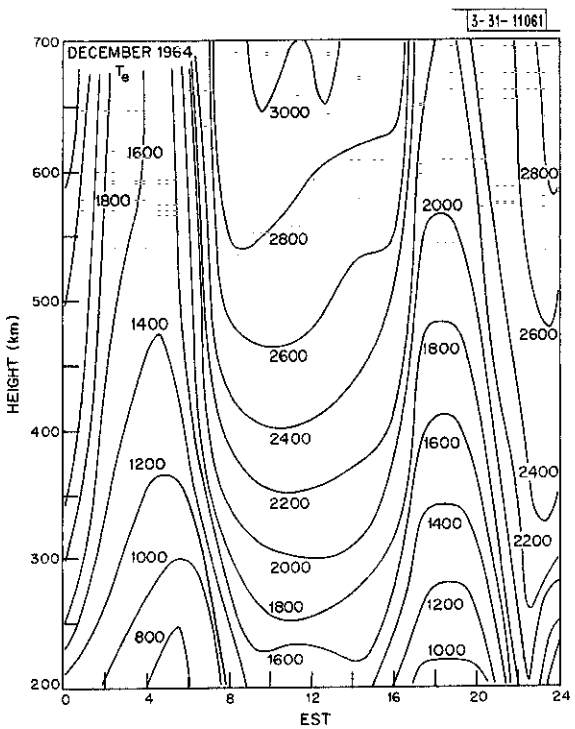

(b) Electron temperature.

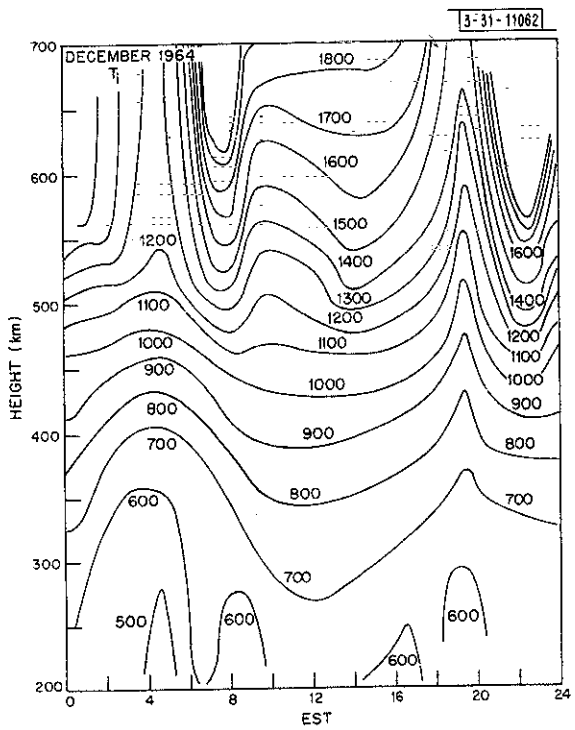

(c) Ion temperature.

Fig. 12. Mean monthly behavior for December 1964.

VI. SEASONAL VARIATIONS

A. Electron Density

Figures 13(a-d) show the seasonal variation in electron density at midnight, 0600, noon and 1800 hours, respectively. No smoothing has been applied to these diagrams or the other plots showing seasonal variations (below) in contrast to Figs. 1(a-c) – 12(a-c).

At midnight [Fig. 13(a)] the peak densities are higher in summer than in winter. In large measure this arises because the sunset increase occurs latest in summer months, and the midnight density values reflect the number of hours elapsed since sunset. What is rather surprising is that the winter values are not actually lower than they are. In part this results from the nocturnal density increase that occurs in winter (Sec. V-A).

Above about 400 km the midnight densities show little seasonal variation. This arises because the higher peak densities (in summer) are offset by lower electron density scale heights arising from lower electron (and ion) temperatures.

In all seasons the electron temperature begins to rise at about ionospheric sunrise ($\chi \sim 100°$, see Sec. VIII), i.e., 40 to 50 minutes before the electron density begins to increase, which occurs at about ground sunrise.

Table II gives the time of ionospheric sunrise and it can be seen that this occurs before 0600 in summer and later than this time in winter. The seasonal variation shown in Fig. 13(b) is chiefly a consequence of this effect. Because the density is rising extremely rapidly at 0600 in the equinoctial and summer months, the contours shown in Fig. 13(b) for these times may be somewhat in error, and the May peak is perhaps an artifact of the plots from which this graph was constructed. The noon behavior [Fig. 13(c)] illustrates clearly the so-called seasonal anomaly, of higher values of f_oF2 in winter than in summer. It is striking that the anomaly is strictly a feature of the peak of the layer. At an altitude of about 400 km or above, highest densities tend to occur in the equinoxes, and it is evident from Fig. 13(c) that the total content $\int_{200}^{700} N\,dh$ is a maximum at these times. This is confirmed by Faraday rotation measurements.[17] Thus, the high values of f_oF2 in winter arise as a result of greater densities near the peak of the layer which are not reflected in the profiles substantially above h_{max}. That is, the density decrease immediately above the layer is faster in winter than at any other time. This is shown most clearly in Fig. 14 where we have plotted the height interval required for the density to fall from N_{max} to a value 0.7 N_{max} above the peak. The figure shows the mean monthly variation of this thickness parameter at noon in 1964. The two profiles nearest noon on each of the days listed in Table I were used to compute the mean and the error bars are probable errors derived from the scatter of the values. It can be seen that there is only an annual variation in this parameter, the minimum being in winter.

The parabolic semithickness of the lower part of the layer also varies smoothly from a summer maximum to a winter minimum.[18] This striking change in layer shape has also been demonstrated by the seasonal variation in the "slab thickness" parameter [= $(\int N\,dh)/N_{max}$] determined from Faraday rotation measurements.[17] Thomas[19] has discussed the changes in layer shape that might result from changes in T_e, T_i or T_e/T_i, and found that these are small. The temperature results presented in the following sections show that there is little seasonal variation in T_e, T_i or T_e/T_i. Thus the seasonal variation of the slab thickness apparently does not arise as a consequence of large changes in T_e and T_i as suggested by Yeh and Flaherty.[17]

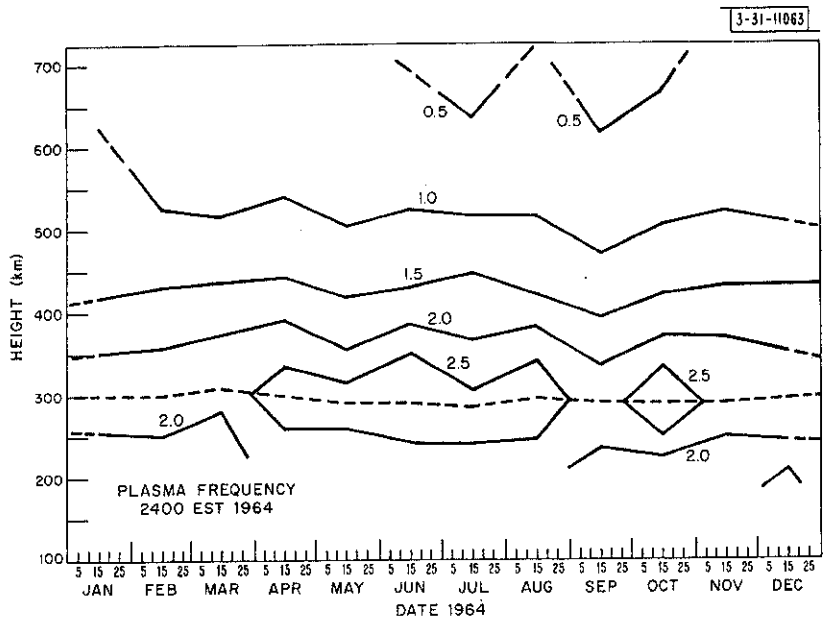

(a) At midnight.

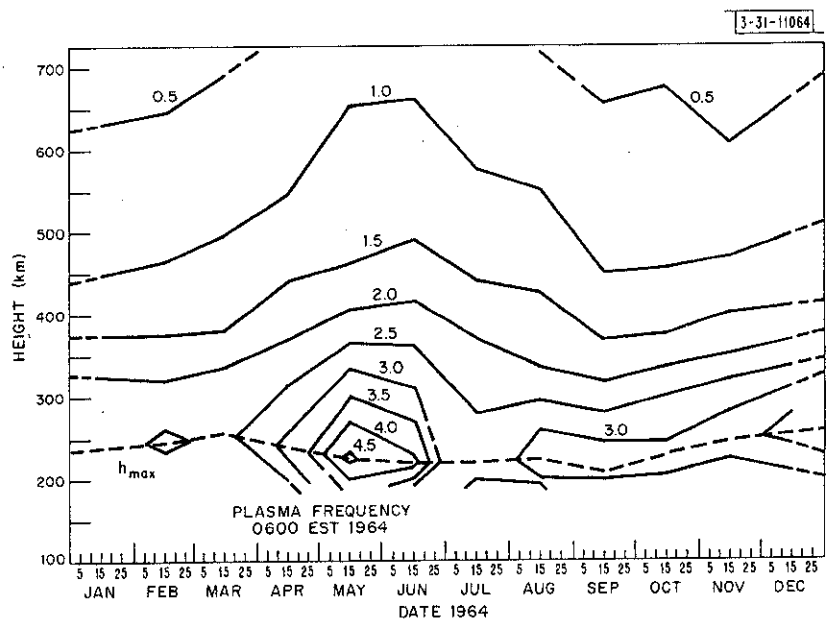

(b) At 0600 hours.

Fig. 13. Seasonal variation of plasma frequency.

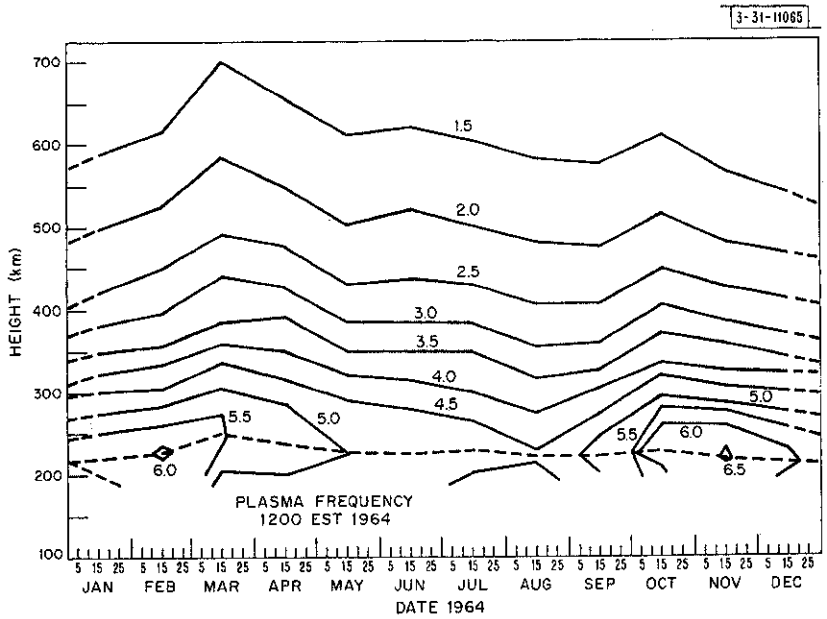

(c) At noon.

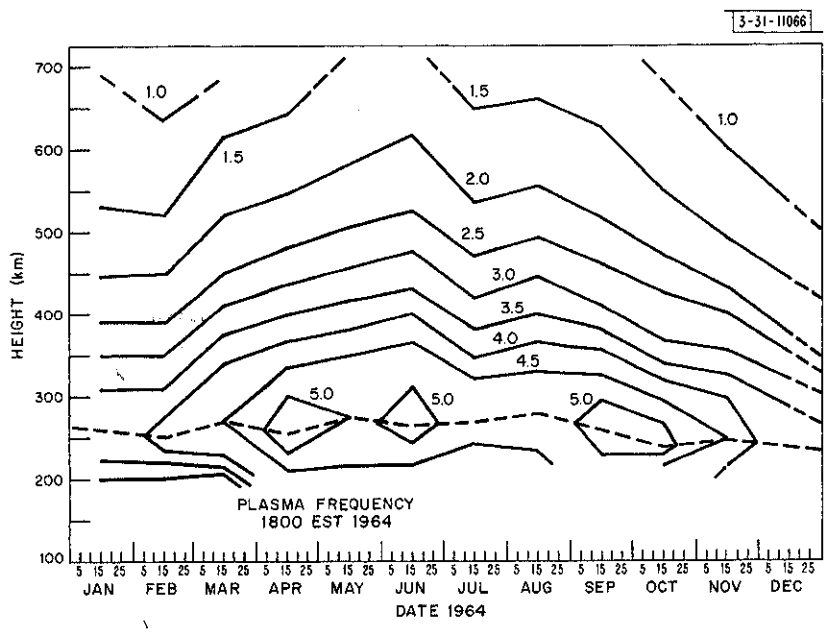

(d) At 1800 hours.

Fig. 13. Continued.

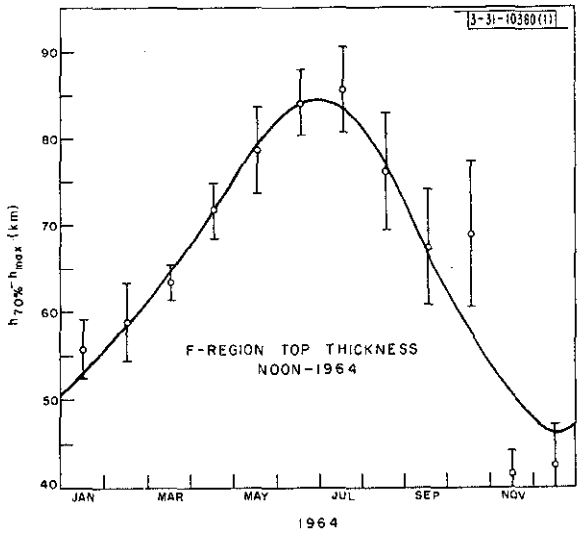

Fig. 14. Seasonal variation of the thickness parameter $h_{70\%} - h_{max}$.

The sunset increase in density is an observable phenomenon only in summer and equinoctial months. The electron temperature begins to decrease some 30 or so minutes before ionospheric sunset (Table II) and the electron density increase which follows reaches a peak at about ionospheric sunset. Thus the equinoctial maxima shown in Fig. 13(d) arise simply as a result of the fact that the sunset increase is occurring near 1800 hours. In summer it occurs later and in winter not at all.

B. Electron Temperature

Because the variation of electron and ion temperature with time tends to be small near noon and midnight [Figs. 1(b, c) to 12(b, c)], we have taken 6-hour averages centered on these times.

Figures 15(a-b) show the variation of the mean daytime (0900 to 1500) and mean nighttime (2100 to 0300) electron temperatures. The daytime results [Fig. 15(a)] show no pronounced seasonal variation below 300-km altitude. Above 300 km there appear to be real variations, for example, a summer minimum and equinoctial maxima, as noted in 1963 (Ref. 2). At night there is a very pronounced seasonal trend. The temperatures are lowest in summer (June and July) and increase uniformly into the winter. As noted in Sec. V, this is thought in part to be a consequence of a higher protonospheric heat flux due to the fact that the conjugate ionosphere remains sunlit in winter. Also, fast photoelectrons arriving from the conjugate ionosphere serve to heat the local ionosphere in winter but not in summer (Sec. VII).

C. Ion Temperature

The comments made above for electron temperature can partly be applied to the ion temperature shown in Figs. 16(a-b). The daytime averages show no seasonal trend, but at night the temperatures are clearly highest in winter and lowest in summer. The summer-to-winter difference in T_i at night is considerably less than for T_e, indicating that the latter is a far better indicator of nocturnal heating. No good explanation can be offered for why the nighttime temperature is so low in August [Fig. 16(b)]. The magnetic activity on the days of observation in this month (Table I) was not particularly different from that encountered in any other month.

D. Electron-to-Ion Temperature Ratio

Figures 17(a-b) show the variations of T_e/T_i over the year. As may be expected from the foregoing, the daytime values [Fig. 17(b)] show no pronounced seasonal variation, while at night the lowest values are encountered in summer and the highest in winter. The peak daytime value [Fig. 17(a)] is somewhat higher than the peak value reported previously.[2] This is because the computed spectrum profiles employed for comparison in 1963 were inaccurate (Sec. III). The peak always lies between 300 and 350 km, irrespective of season, and has a value in the range

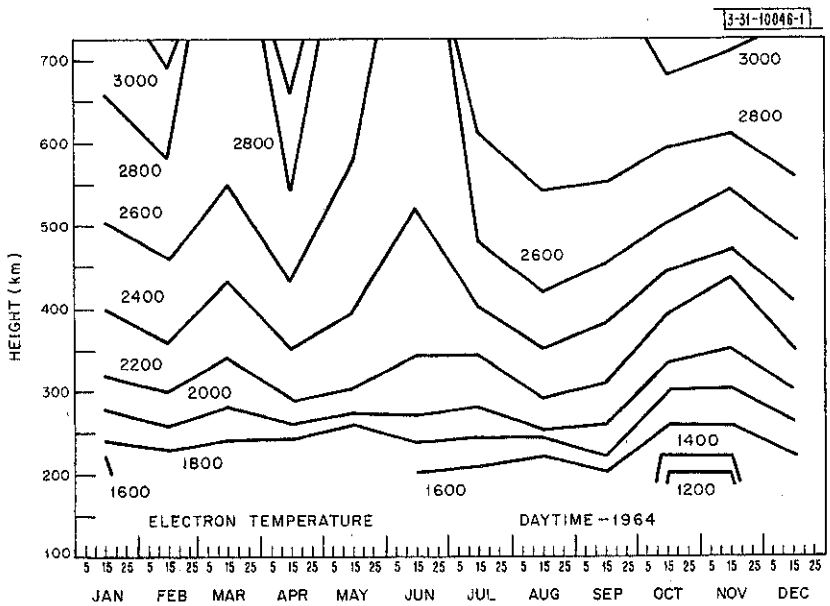

(a) Average daytime (0900 to 1500 hours).

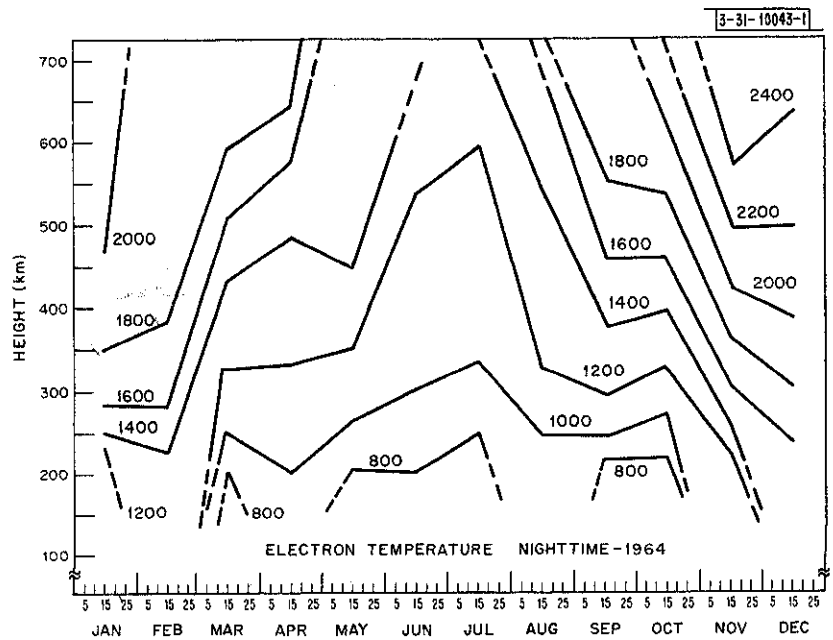

(b) Average nighttime (2100 to 0300 hours).

Fig. 15. Seasonal variation of electron temperature.

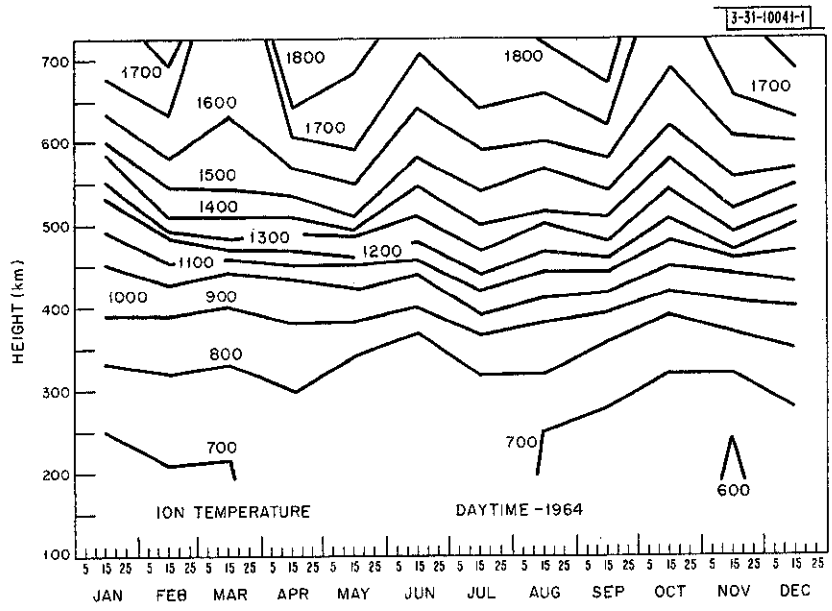

(a) Average daytime (0900 to 1500 hours).

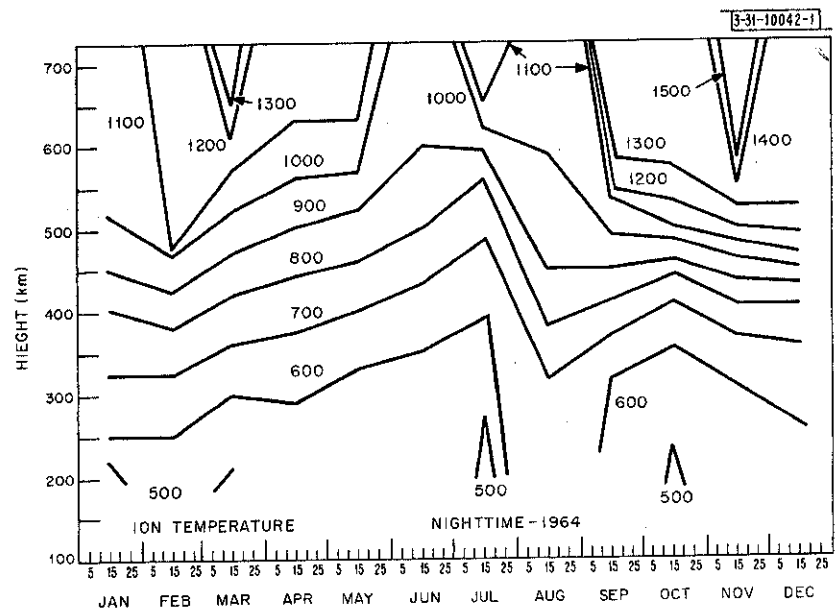

(b) Average nighttime (2100 to 0300 hours).

Fig. 16. Seasonal variation of ion temperature.

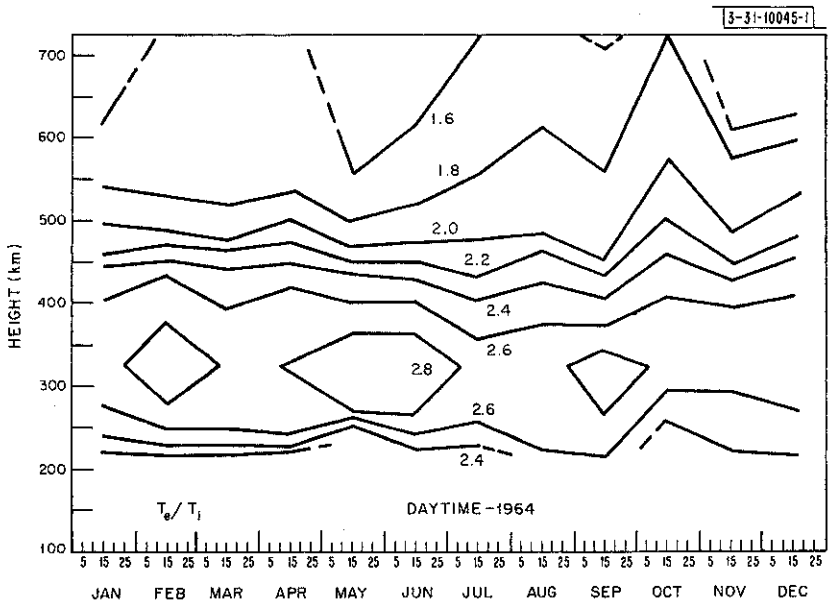

(a) Average daytime (0900 to 1500 hours).

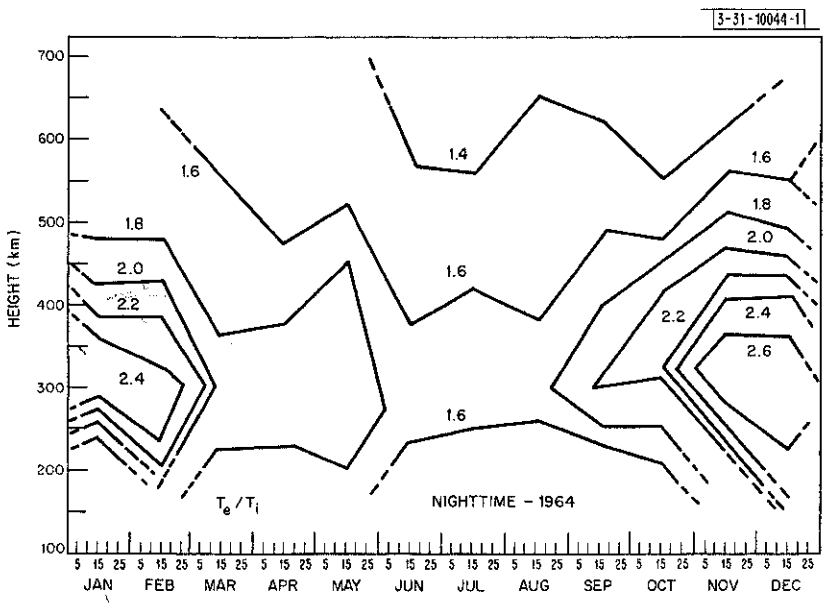

(b) Average nighttime (2100 to 0300 hours).

Fig. 17. Seasonal variation of T_e/T_i.

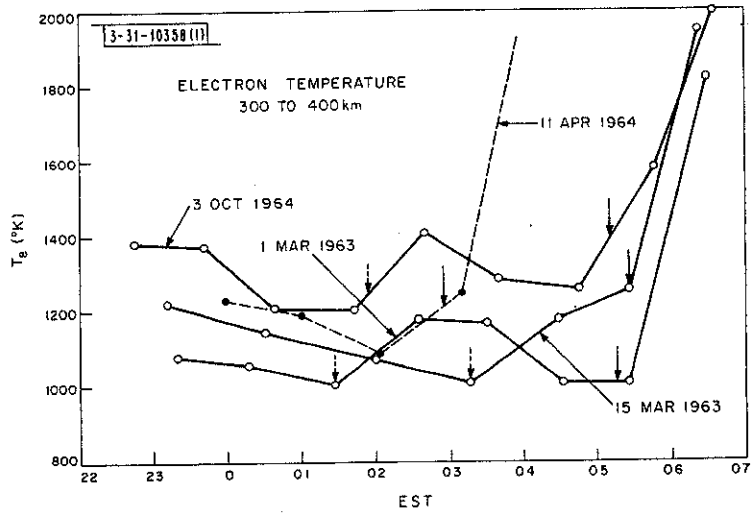

Fig. 18. Variation of T_e showing predawn increases coincident with conjugate sunrise. Solid arrows indicate time of onset of local heating as estimated from $\Delta T_e/dt$ and broken arrows indicate time at which conjugate point heating commences.

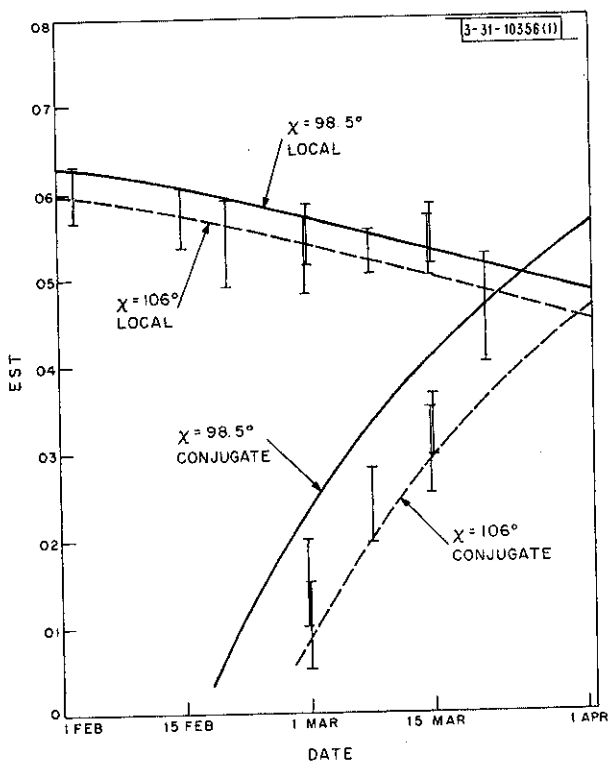

Fig. 19. Times at which local and conjugate sunrise heating appears to commence (Fig. 18). Time at which sun's zenith distance is 106° and 98.5° is also indicated. These two angles correspond to earth's shadow, reaching 200 and 100 km, respectively.

from 2.6 to 3.0. At 600-km altitude T_e/T_i has declined to about 1.6. At night the peak is found to lie at about the same altitude, but has a value which varies markedly with season – about 2.6 to 2.7 in winter and 1.6 to 1.7 in summer. However, at 600 km the variation is less – from about 1.4 in summer to about 1.6 in winter.

VII. PHOTOELECTRONS FROM CONJUGATE IONOSPHERE

In Ref. 2 we drew attention to a predawn increase in electron temperature occurring in March. Since that time Carlson[20-22] has shown that the phenomenon is a regular feature of the early morning behavior throughout the winter months at Arecibo, and demonstrated that the source of this heating is a flux of fast photoelectrons streaming from the conjugate ionosphere following sunrise in that hemisphere. The onset of the heating has been found to coincide with a solar zenith distance of $\chi = 98°$ to 99° at sunspot minimum when the temperature in the height range from 300 to 400 km is used as an indicator. Heating associated with local sunrise is found to occur at the same zenith distance. Toward sunspot maximum, the zenith distance χ at which heating effects are first noticed increases owing to the greater expansion of the atmosphere.[23]

A search has been made for evidence of heating at Millstone Hill coinciding with sunrise at the conjugate point. The phenomenon cannot be expected at Millstone in winter since the conjugate point then remains sunlit even at ground level throughout the day (Table II), and it is not readily possible to distinguish between heat conducted from the protonosphere, and a photoelectron flux. Because the conjugate point to Millstone lies south of the Antarctic Circle and about 36 minutes of time farther west than Millstone,[4] there is a sunrise (i.e., χ reaches 98° to 99°) at the conjugate point which precedes local sunrise only on about 30 days each equinox. However, an examination of the temperature results obtained during these 30-day periods in 1963 and 1964 does provide evidence for the onset of heating coinciding with conjugate sunrise. Figure 18 shows the electron temperature obtained by averaging values obtained for 300 and 375 km observed on a number of days during these selected periods. The time resolution (~1 hour) in these measurements allows one to distinguish between local and conjugate heating only when the two sunrises are separated by more than about two hours. We have attempted to indicate in Fig. 18 the times at which we estimate that conjugate and local heating commenced. On 11 April there is only a single abrupt change in $\Delta T_e/dt$ – that associated with local sunrise. On 15 March the temperature begins to rise (at ~2°/min.) approximately 2 hours before local sunrise and continues to do so until local sunrise when there is another abrupt increase ($\Delta T_e/dt \sim 12°$/min.). This behavior is similar to that reported by Carlson[20-22] for Arecibo ($L \sim 1.4$). At Millstone ($L \sim 3.2$) it is possible for conjugate sunrise to precede local sunrise by as much as 4 to 5 hours. In this case the temperature appears to rise, reach a peak and then decline to its earlier level (as on 1 March 1963, 3 October 1964). This is distinctly different from the behavior reported[24] by the French group at Nancay ($L \sim 1.8$), where, following conjugate sunrise, the ionosphere is soon heated to almost its full daytime value, and local sunrise causes no perceptible increase in T_e. The difference in the behavior at Millstone and Nancay might be attributed to the shorter field line length for Nancay, with consequent greater transparency to the fast photoelectrons.

In order to establish that nocturnal increases of T_e observed during these equinoctial periods are associated with conjugate sunrise, we have plotted in Fig. 19 the times of occurrence, together with the time at which $\chi = 98.5°$ at the local and conjugate points. As remarked previously, the poor time resolution afforded by the present measurements does not permit the

precise time of the onset of heating to be established, and the bars in Fig. 19 indicate the range of uncertainty. It would appear that both local and conjugate heating commence slightly before a zenith distance $\chi = 98{\cdot}5°$ is reached, and that the true value probably lies between $\chi = 100°$ and $\chi = 106°$. However, a small shift in the assumed latitude of the conjugate point would make a large change in the value of χ at which conjugate heating would appear to commence.

Theoretical studies of the behavior of the electron temperature during sunrise have been made by da Rosa[25] who finds that T_e begins to increase as χ reaches 110°. In this analysis the heat input to the electron gas was assumed to be a Chapman function below 300 km and the Geisler-Bowhill model of midday nonlocal heating[26] was assumed above. This seems rather arbitrary as the shadow of the earth's atmosphere must be well above 400 km at $\chi = 110°$ and exact calculations would be required to estimate what effect this must have on the fast photoelectron flux.

VIII. DISCUSSION

A number of authors have sought to explain the seasonal anomaly in terms of temperature variations of the atmosphere. The lowest critical frequency values were encountered in August and the highest in November and December. When comparing Figs. 15(a), 16(a), and 17(a) with Fig. 13(c), we find that there does seem to be some correspondence between density and temperature during the period from July to December. The electron temperature at the peak of the layer decreases by ~200°K from summer to winter and at 300 km the decrease is ~300°K. The ion temperature decreases by about 100°K in this height interval. These variations do not seem to be supported by the results for the first part of the year. The only parameter that definitely shows a variation correlated with f_oF2 is T_e/T_i at h_{max}. However, the variation is small — from 2.4 in summer to 2.6 in winter.

The absence of major daytime seasonal variations in these quantities [Figs. 15(a) and 17(a)] shows that an explanation for this seasonal variation of layer thickness[17,19] in Fig. 14 (by almost a factor of two) must be sought elsewhere. The neutral temperature T_n is a maximum in the solstices and a minimum in summer and winter,[27] and hence variations in T_n cannot be invoked as an explanation either. Thus, it appears impossible to invoke temperature changes which result in either changes of the height distribution of the constituents or the reaction rates of the loss processes[28] to explain the seasonal anomaly.

IX. 23-CM OBSERVING PROCEDURE

The parameters of the 68- and 23-cm radar systems are given in Table III. It can be seen that the 23-cm radar is of the order of 7 db less sensitive than the 68-cm system. This is chiefly a consequence of the smaller (84-foot diameter) antenna employed for the higher frequency radar. The antenna used with the 23-cm radar system employs a Cassegrainian feed arrangement and is mounted on a 90-foot pedestal. It can be driven in azimuth and elevation at speeds of 4°/sec, but in these observations it was left in one position. The receiver employs four diode parametric amplifiers in cascade as first amplifying stages, and following two stages of frequency conversion the signals are applied to the IF amplifiers of the 68-cm receiver. From this point on, all the operations applied to the signals are the same as carried out with the 68-cm radar and described previously.[1] One change that must be made when operating at 23-cm wavelength is the insertion of a new set of crystal filters in the spectrum analyzer. The spectral width of the echoes would be expected to be approximately three times wider owing

TABLE III

RADAR SYSTEMS EMPLOYED AT MILLSTONE HILL FOR IONOSPHERIC BACKSCATTER STUDIES

Location	71.5°W 42.6°N	71.5°W 42.6°N
Antenna beamwidth	0.7°	0.6°
Polarization	Circular	Circular
Effective aperture	1600 m^2	190 m^2
Frequency	440 MHz	1295 MHz
Peak transmitter power	2.5 MW	4 MW
Transmitter pulse lengths	0.1, 0.5, 1.0 msec (other values are possible for each)	0.5 msec
Pulse repetition frequency	40 Hz	40 Hz
System temperature	250°K (monitored continuously for each)	~170°K
Postdetector integration	~20 db	~20 db
System losses	~1 db	~2 db

to the higher operating frequency employed, but since most of the 23-cm observations refer to heights below 200 km where the ion temperature is lower and the mean ionic mass is higher, the spectral width of the reflected signals is not increased by such a large factor. (The center to half-peak width encountered is usually in the range from 8.0 to 15.0 kHz.)

When used to observe the E- and F_1-regions of the ionosphere, the radar is operated with the antenna tilted so that the zenith distance of the beam is of the order of 60° to 80°. In this way it is possible to place the echo from the E-region at a delay greater than the interval occupied by the ground-clutter echoes. For a pulse of fixed length, the height Δh illuminated decreases with increasing zenith angle χ, thereby improving the height resolution achieved. The penalty one must pay for this is a reduction of the signal strength since, for a radar system in which the scatterers fill the beam, the echo intensity falls as the square of the range to the scattering volume.[1] A further constraint imposed upon the pulse length τ (by the method of making spectrum measurements at Millstone Hill) is that the spectral width of the pulse ($1/\tau$ Hz) must be considerably less than the spectral broadening $[\langle |H(\nu t_o)|^2 \rangle_{avg}$ in Eq. (2)] introduced by the ionosphere, if accurate temperature and composition measurements are required. Finally, in a given location the range spread of the ground-clutter echoes will depend directly upon τ and may, in addition, depend upon the zenith distance χ (and bearing) of the antenna.

In the work reported here, a zenith distance $\chi = 70°$ and pulse length $\tau = 0.5$ msec ($\Delta h \approx 30$ km) were employed. This zenith distance was the minimum required to place the E-region echo beyond the ground clutter when using this pulse length. For this value of χ a 6-db reduction of echo power is encountered relative to making the observations in the zenith with the same height resolution. The choice of pulse was determined by the sensitivity requirement. Given a more powerful radar system the pulse could be shortened to about 0.2 msec (yielding $\Delta h \approx 12$ km at $\chi = 70°$) before the constraint relating the spectral width of the pulse to that of the medium is reached. Even with a 0.5-msec pulse it was not possible to obtain useful measurement at night

or near sunrise or sunset when the electron concentration is low. Thus the results reported herein apply only to daytime conditions. The height resolution achieved (Δh = 30 km is considerably less than might be desired, but it is far better than is achieved with the 68-cm radar temperature measurements at F_2-region heights (Δh = 75 km).

Table IV lists the days and times in 1966 on which observations were made. The spectrum analyzer was employed to examine the signal spectra at delays of 1.5, 2.0, 2.5, . . . 5.0 msec along the time base.

TABLE IV

IONOSPHERE OBSERVATIONS USING THE 23-CM RADAR IN 1964

Date (1964)	Commencement (EST)	End (EST)	Height/Range Examined (km)
16 April	1000	1600	80-260
13 August	0900	1600	80-230
10 September	0900	1500	80-230
25 September	0900	1500	80-230
9 October	0900	1500	80-290
23 October	1200	1530	80-230
5 November	1000	1600	80-260
20 November	0900	1630	80-260

On many days the signals were too weak to permit useful spectral measurements at delays of 4.5 or 5.0 msec. Thus the height interval over which signal spectra could be obtained is shown for each day in Table IV. For each position of the sampling on the time base the integration was allowed to proceed for five minutes, and thus it usually required about an hour to examine all the delays in the range from 1.5 to 5.0 msec, and typically the entire range would be sampled 6 or 7 times in a given day.

The spectra obtained were subsequently plotted and scaled to yield the ratio x between the amplitude in the wing to that at the center and f the half-peak-power width. No marked diurnal variation of these quantities was evident, and since the spectra were, in general, weak and difficult to scale, an average was computed for x and f for each height interval on any one given day.

X. 23-CM DATA REDUCTION

A. Problem of Mixtures of Ions

In the height interval from 100 to 200 km, the composition of the ionosphere changes. At low altitudes O_2^+ and NO^+ ions predominate, but higher up O^+ is the principal ion.[29] While it is possible in principle to determine both the composition and temperature from backscatter radar observations for mixtures of O^+ and H^+ (or He^+) ions encountered near 1000 km[6] this is not the

case for mixtures of O^+, O_2^+, and NO^+ ions. Not merely is it impossible to distinguish O_2^+ from NO^+ ions, but one cannot determine the ratio of the light (that is, O^+) ion abundance to the heavy (that is, $O_2^+ + NO_2^+$) ions without additional information concerning the temperature.[30] Stated otherwise, it is possible to recover an almost identical signal spectrum following a change in the relative abundance of these ions by a suitable change in the electron temperature T_e and ion temperature T_i. Accordingly, one can use the data to determine composition and electron (or ion) temperature but not all three, and in order to obtain results for two of the unknown it is necessary to make an assumption concerning the third. The most acceptable assumption, on the basis of present knowledge, is that the ion and neutral temperatures are the same in the interval from 100 to 200 km.[26,31,32] One may then adopt a profile of neutral temperature based upon satellite drag data or, as was done in the present instance, determine directly the exospheric temperature T_{ex} of the neutral atmosphere from the uppermost spectra, which correspond to altitudes (230, 260, or 290 km) where only O^+ ions may be presumed to be present. It is then necessary to assume only some altitude dependence for T_i (= T_n) for all lower heights. The one that was adopted here is the exponential dependence

$$T_N = T_{ex} - (T_{ex} - 355) \cdot \exp[-0.0156(h - 120)] \qquad (8)$$

implied by the 1965 CIRA model atmosphere for the Models I and II ($\overline{F}$ = 65 and 75 × 10^{-22} $W/m^2/Hz$, respectively), which correspond most closely to the solar flux conditions encountered during these observations. In sum, Eq. (8) defines the neutral temperature T_n as a function of the height h above the earth (in kilometers) with only one unknown T_{ex}. By determining the ion temperature at any height in the interval from 250 to 300 km, T_{ex} will be fixed. Where spectra were obtained at more than one altitude in this height range (16 April, 9 October, 5 November and 20 November), it is possible to obtain more than one estimate of T_{ex}. In such instances the agreement found was invariably good, and this lent some confidence to the procedure adopted.

In passing, it may be noted that it is possible to assume some dependence of composition upon altitude and then deduce T_e and T_i. This approach has been adopted in the reduction of data obtained by the French group at the Centre National d'Etudes des Telecommunications.[24] However, such an approach is open to the objection that the ion composition has been measured in only an extremely limited number of rocket flights (Fig. 20). In addition, on theoretical grounds[33] we would expect the composition to exhibit diurnal changes, and experimental evidence for this has been obtained by Istomin,[34] as illustrated in Fig. 21, and Holmes, et al.[35]

B. Electron Temperature T_e

When the ion temperature has been determined at all altitudes by the procedure outlined above, the electron temperature can be estimated from the shape of the signal spectrum without any knowledge of the ion composition. This follows from the fact that the ratio x between the peak power in the wing of the spectrum and that in the center primarily depends upon the ratio T_e/T_i.[6] However, for precise results it is necessary to take into account the actual value of T_i as well as the composition. Figure 22 shows the variation of x with T_e/T_i for the temperature range 400°K < T_i < 1400°K for mixtures of 100% O^+, 100% NO^+ and 50% O^+, 50% NO^+ computed for a radar frequency f = 1295 MHz, pulse = 0.5 msec, and plasma frequency f_N = 10 MHz. It can be seen that although the results will not be wildly in error if a mean curve is drawn through the shaded regions of Fig. 22, somewhat better results will be obtained if some model

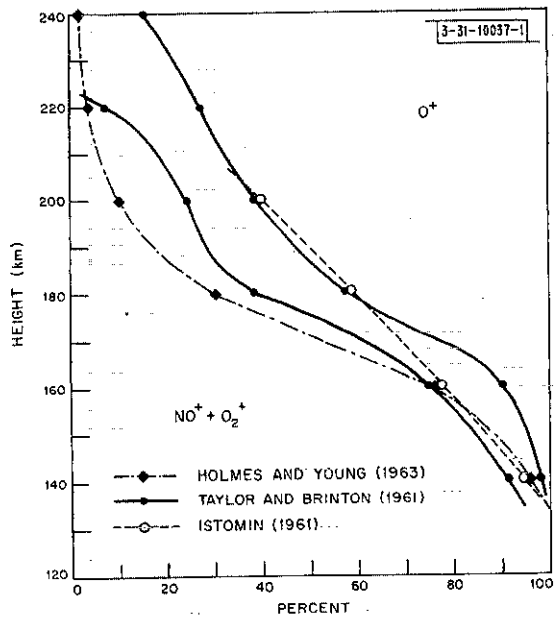

Fig. 20. Rocket profiles of relative abundance of O^+ and sum of O_2^+ and NO^+ ions by three workers.

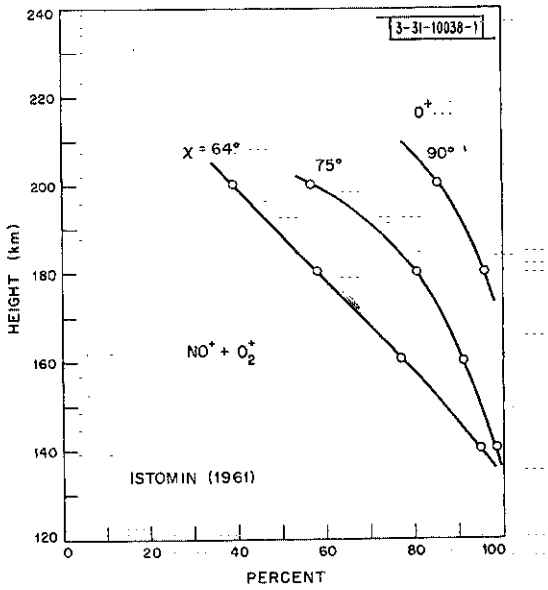

Fig. 21. Variation of abundance of light-to-heavy ions with solar zenith distance, according to Istomin.[34]

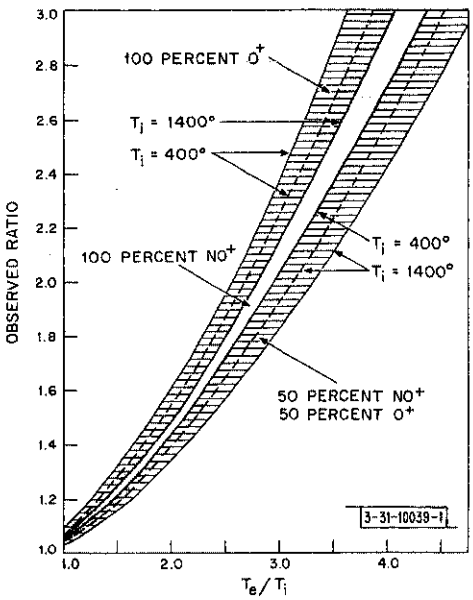

Fig. 22. Variation of ratio x of power in wing of spectrum to that at center frequency as a function of T_e/T_i for three compositions, and range of ion temperatures of 400 to 1400°K. It can be seen that because spread is not large electron-to-ion temperature ratio T_e/T_i can be determined at least approximately irrespective of ion temperature T_i or composition.

TABLE V

MODEL FOR VARIATION OF T_e/T_i, T_i, AND COMPOSITION WITH ALTITUDE

Altitude (km)	T_e/T_i	T_i	O^+ (%)
130	1.0	435	0
170	1.5	660	45
200	2.0	715	58
230	2.5	750	100
⩾270	3.0	800	100

for the variation of T_i, T_e/T_i and composition with height is adopted. In the event that the model is not in good agreement with the results obtained, a revised model may be tried. The model finally adopted on the basis of the observations in 1964 is presented in Table V. Using this model a single curve relating x and T_e/T_i was drawn (Fig. 23) from which all the values of electron temperature were derived.

It should be noted that as T_e/T_i, T_i, and the percentage O^+ composition all increase with height from what are initially low values, it is difficult to change the model significantly and thereby appreciably alter the values of T_e obtained below about 175 km. At 230 km and above it has been assumed that only O^+ ions are present, and thus at this altitude T_e/T_i can be determined without recourse to the model. It follows that the model does not, in fact, influence the results for T_e/T_i significantly at any altitude. The choice of curve in Fig. 23 does influence the values of composition reported here. In practive, however, it is not possible to employ a model that differs significantly from that given in Table V and obtain results that then support the model (see Secs. X-D and XII-A).

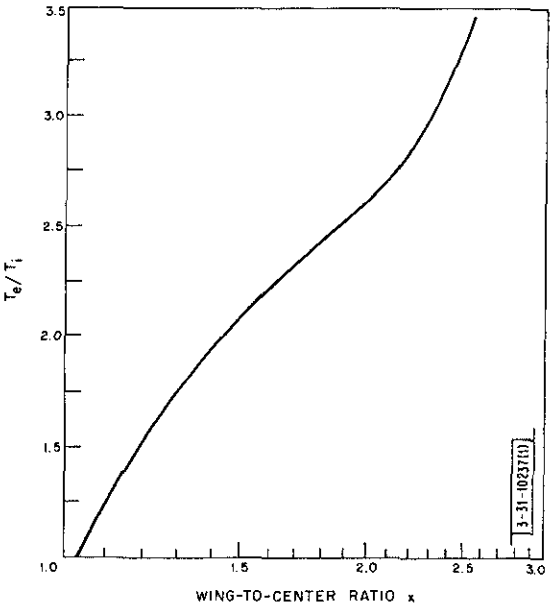

Fig. 23. Adopted variation of T_e/T_i with ratio x between power in wing of spectrum to that at center frequency. This curve corresponds to model for variation of T_e/T_i, T_i, and composition with height assumed (Table V) which is in good agreement with results later obtained.

C. Ion Composition

To analyze the observed spectra, a set of theoretical spectra were computed, using the equations given by Fejer[5] for the following cases: T_i = 400 to 1600°K in 200° steps, T_e/T_i = 1.0 to 4.0 in 0.25 steps, percentage O^+ = 0 to 100 percent in 25-percent steps. (The other ion was taken to be NO^+.) These spectra were then convolved [Eq.(2)] with the weight function that represents the combined (instrumental) effect of transmitting a pulse and gating from the radar time base a section equal in length to the transmitted

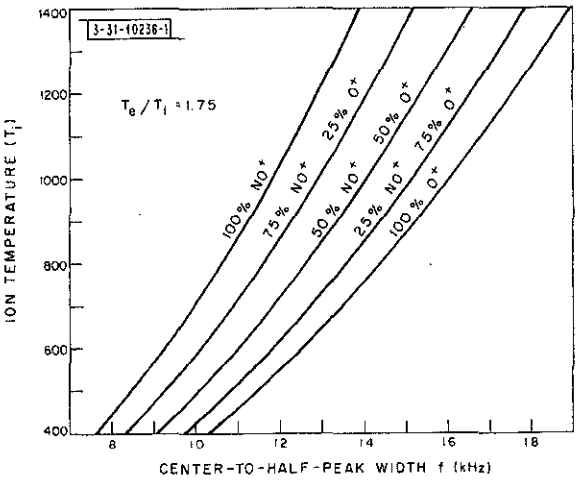

Fig. 24. Variation of spectral width f as a function of ion temperature (along ordinate) for different compositions and fixed value of T_e/T_i (= 1.75). These curves can be used to determine composition by interpolation given T_i and f.

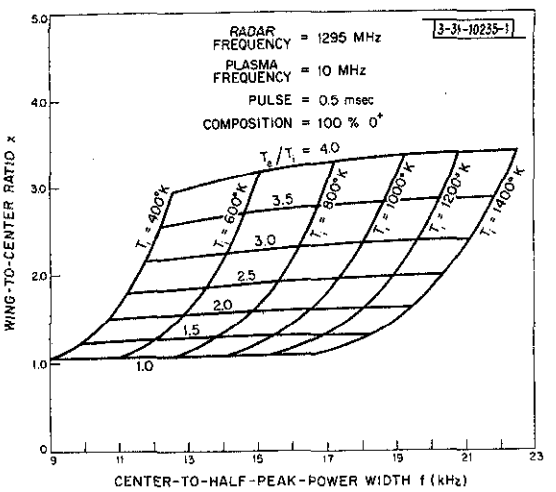

Fig. 25. Variation of spectral width f and wing-to-center ratio x as a function of ion temperature T_i and electron-to-ion temperature ratio T_e/T_i for case of only O^+ ions present. These curves can be used to determine T_i and T_e/T_i for spectra obtained for altitudes above 220 km and below about 600 to 800 km. Spectra obtained in the height interval 230 to 290 km were analyzed using this chart and thereby yielded estimates of neutral exospheric temperature T_{ex}.

pulse. This function was then convolved [Eq. (1)] with the spectral function of the filters employed in the receiver spectrum analyzer.

A set of curves was next prepared showing the variation of the spectral width f as a function of T_i for a given ratio T_e/T_i. In all, there were five curves representing the five compositions chosen for each case of T_e/T_i. Figure 24 represents an example of one of these diagrams. In addition, a chart showing the variation of T_i and T_e/T_i as a function of x and f (Fig. 25) was prepared for the case of only O^+ ions present. Using this chart (Fig. 25) and the values of x and f for the uppermost spectra (230-, 260- and 290-km altitude), T_i and T_e/T_i at the corresponding heights are determined. For each value of T_i the exospheric neutral temperature T_{ex} is determined from Eq. (8) and a mean is taken when more than one value is obtained. The value of T_i (= T_n) at all lower altitudes is then obtained from Eq. (8). Next, T_e/T_i is obtained for each altitude from the ratio x, using Fig. 23. The value of T_e/T_i obtained determines which chart (e.g., Fig. 24) closest to the measured value is selected. A point representing the observed value of f and the deduced value of T_i is then entered on this chart, and by interpolating between the curves the percentage of O^+ ions and percentage of $[O_2^+ + NO^+]$ are found. In most cases the measured value of T_e/T_i was not precisely the same as on any chart, and it was necessary to interpolate between the values of composition deduced from adjacent charts.

D. Checks on Results

A number of tests can be applied to see if the results are reasonable, quite apart from any comparison with rocket or other data. As noted above, when it has been possible to deduce T_{ex} from spectra at different delays, we require that they should each give the same value. Failure to do so would most likely indicate a significant number of NO^+ ions at 230-km altitude. Next, we may examine the lowest spectra, assuming that only NO^+ ions are present, and compare the ion temperature so derived with that deduced in the manner outlined above. No large differences should be expected. Further, when interpolating to obtain the composition (Fig. 23) there is no a priori reason why ratios of more than 100% NO^+ (or O^+) should not be required by the values of f and T_i inserted. In other words, if reasonable compositions are obtained, one derives confidence in the approach adopted, because sensible values are in no way forced to result from the method of analysis. Finally, the temperatures obtained above 200-km altitude may be compared with values obtained (albeit on different days) with the 68-cm vertically directed radar.

XI. 23-CM RESULTS

A. Exospheric Temperature T_{ex}

While it is not the main objective of the experiment to determine T_{ex}, it is instructive to compare these radar values with ones obtained from satellite drag observations. This is done in Table VI where satellite drag determinations of T_{ex} kindly furnished by Dr. L. G. Jacchia of the Smithsonian Astrophysical Observatory are given. The latter are averages of the seven-hour values spanning the time period 0900 to 1500 EST for the latitude of Millstone. Although the two sets of values do not show strikingly good agreement, they are not in violent disagreement. The satellite values are on average some 40°K (i.e., 5 percent) higher than the radar values. If the satellite values are regarded as "true," then the radar values exhibit an RMS error of 71°K (i.e., 9 percent), which seems larger than we would have anticipated (Sec. XII).

TABLE VI

VALUES OBTAINED FOR EXOSPHERIC TEMPERATURE T_{ex}, AVERAGED OVER THE TIME INTERVAL 0900 TO 1500 EST

Date	Radar T_{ex}(°K)	Satellite T_{ex}(°K)	Difference Satellite Minus Radar (°K)
16 April	788	865	77
13 August	759	790	31
10 September	897	815	−82
25 September	807	855	48
9 October	794	890	96
23 October	848	825	−23
5 November	800	880	80
20 November	726	820	94
		Mean Difference =	40

B. Electron Temperature

The lowest altitude to which the electron temperature could be obtained was for a region centered at 136 km. The spectrum obtained at a delay of 2.0 msec (107-km altitude) showed no double-humped appearance, but instead had a single peak, characteristic of Thomson scattering from a plasma when collisions are important.[36] Similar findings have been reported by the French group[24] over the height interval 90 to 110 km. These workers, employing the CNET bistatic radar system were able to estimate the collision frequency in this altitude range after assuming some temperature profile. Their results yield collision frequencies that are about a factor of two higher than accepted values, indicating perhaps that other processes not included in the theory are important in this altitude range. No attempt has been made to compute collision frequencies from the spectra obtained in this work because the height resolution (~30 km) is extremely poor compared with that achieved in the French observations (~3 km).

The temperature results are presented in Figs. 26(a-e). For each month the results have been averaged (where observations were available for more than one day) and have been plotted, together with the mean daytime (0900 to 1500 EST) temperatures obtained during the same month, with the vertically directed radar (Sec. IV). The bars in Figs. 26(a-e) denote the height occupied by the exploring pulse and are not error bars. It will be noted that with the exception of September it is possible to draw smooth curves through the two sets of points with little difficulty. In several instances, e.g., September, October and November, there is a difference between the two sets of points for the ion temperature that is largest near 220 km. This probably reflects the fact that at this altitude the measurement made at 68 cm (beam vertical) is an underestimate, since the pulse is long enough to extend down into regions where O_2^+ and NO^+ are present, yet the spectrum has been interpreted on the assumption that only O^+ ions are present.

(a) April 1964.

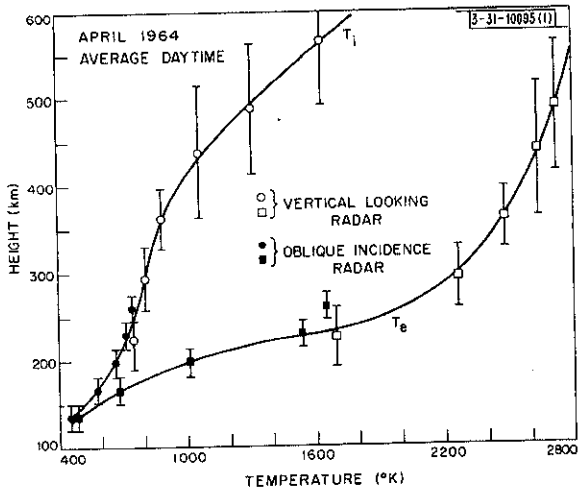

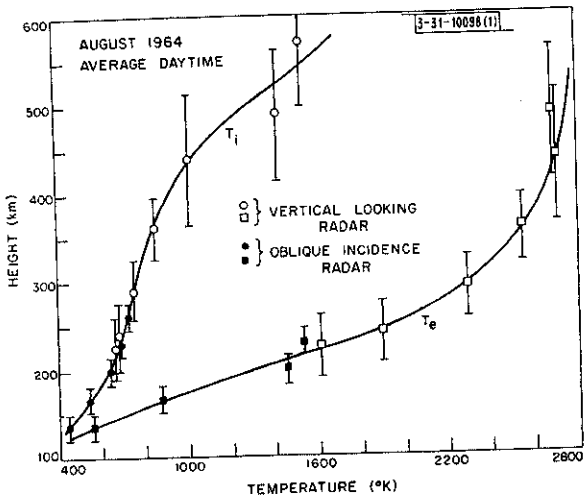

(b) August 1964.

(c) September 1964.

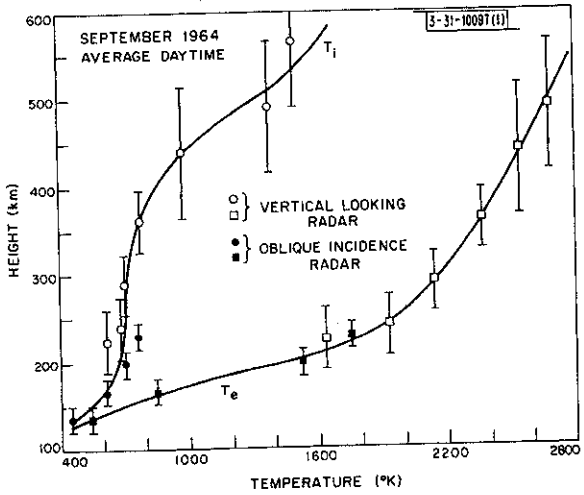

Fig. 26. Average daytime (0900 to 1500 hours) temperature curves obtained with 23- and 68-cm systems.

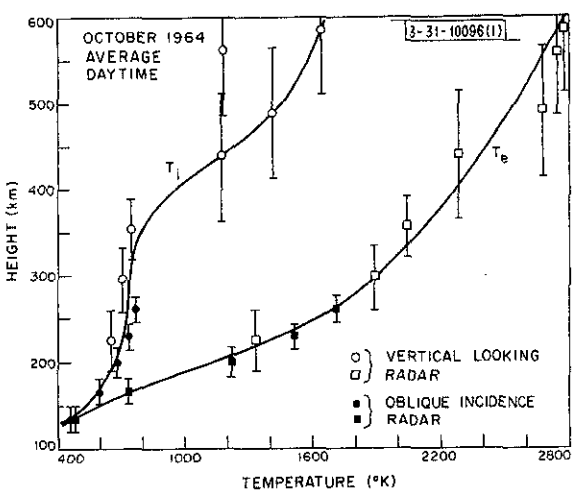

(d) October 1964.

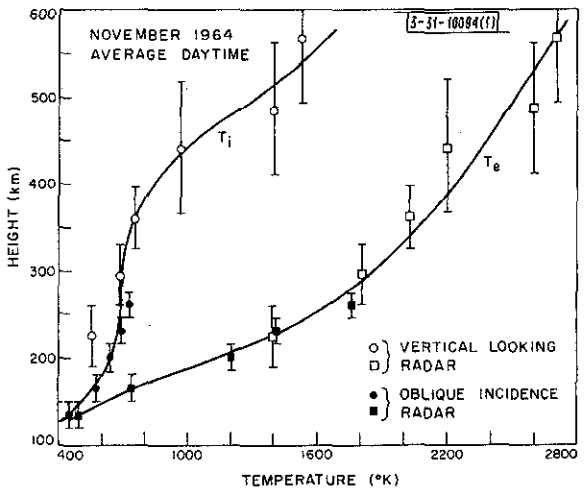

(e) November 1964.

Fig. 26. Continued.

On the basis of the results in Figs. 26(a-e) we may say that at temperate latitudes $T_e > T_i$ (and T_n) at all altitudes above 135 km during the daytime, but that below 120 km it would appear that $T_e = T_i$. This is in agreement with results reported by Carru, et al.,[24] from Thomson scatter observations, but contrary to the conclusion reached by Spencer, et al.,[37] and others from rocket flights. The resolution of this disagreement is awaited with considerable interest, since acceptance of the rocket determinations forces one to conclude that extremely large amounts of solar EUV energy ($\sim 10^5 - 10^6$ eV/cm^2/sec) are absorbed at E-region heights or that some other mechanism is able selectively to heat electrons at these altitudes.[38]

It also appears that $T_i = T_n$ up to an altitude of about 300 to 350 km, above which $T_i > T_n$. This is in good agreement with theoretical estimates of Banks.[31,32] Our results do not extend to sufficiently great heights to determine whether $T_e/T_i \to 1.0$ at about 1000 km as assumed by Hanson[39] and Geisler and Bowhill.[26] The results reported in previous papers[2-4] suggest that at this latitude $T_e > T_i$ for a large range of heights above the F-region, and this too is supported by recent theoretical studies. Banks[31] has shown that the effect of thermal conduction through the ion gas (neglected by Hanson, Geisler, and Bowhill) will be to transport heat downwards from great heights that has been supplied by the electrons via Coulomb encounters. Where the dip angle of the earth's field is sufficiently large, so that the heat conductivity is great enough, the ion temperature will remain below that of the electrons at all altitudes. Thus, above 1000-km altitude at high temperate latitudes, we may expect that the temperatures of the neutrals, electrons and ions are all isothermal, but $T_e > T_i > T_n$.[31,32]

C. Ion Composition

The results for the distribution of the principal ions on the eight days are shown in Fig. 27 together with their mean curve. These results may be compared with rocket determinations (Fig. 20) reported by Istomin,[34] Taylor and Brinton,[29] Holmes, et al.[35] The mean curve of Fig. 27 comes closest to the results of Holmes, et al.[35] (Fig. 20) and indeed the agreement is quite good above 180 km. Below this altitude the radar results indicate fewer heavy ions. It is possible that this discrepancy indicates that the form of the temperature profile adopted [Eq. (8)] is in

error. If this is the case, then we find that at 167 km the temperature must on average be ~90°K higher than given by Eq. (8). Somewhat similar findings have been reported by Spencer, et al.,[37] in rocket determinations of neutral temperature. These indicate that T_n increases with altitude somewhat faster than the Harris-Priester model up to 160 to 170 km and then less rapidly above this altitude.

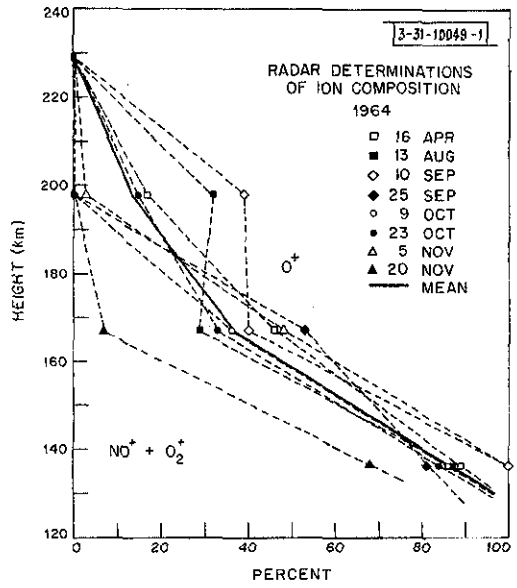

Fig. 27. Relative abundance of O^+ ions and sum of O_2^+ and NO^+ ions as a function of altitude obtained from 23-cm radar results.

XII. DISCUSSION OF 23-CM RESULTS

A. Accuracy

The agreement between the radar and satellite drag determinations of the neutral particle exospheric temperature has been examined in Sec. XI. By averaging the data over the whole day we have sought to minimize the random errors of measurement, yet it remains true that the uppermost spectra that give rise to T_{ex} are the poorest. A crude estimate can be made of the accuracy in determining the ion temperature from the spread of the individual values on a given day. This suggests that individual values are accurate to better than ±10 percent and is almost certainly an underestimate, since it assumes no diurnal variation.

The largest uncertainty in both the composition and the electron temperature determinations is introduced by the assumption of the complete absence of O_2^+ or NO^+ ions at heights in the interval from 230 to 290 km. This is in agreement with some of the rocket determinations (Fig. 20) and in disagreement with others. In the most recent direct measurements,[40] a retarding potential analyzer mounted on an oriented satellite was employed and results have been published for one orbit during which the percentage of $O_2^+ + NO^+$ ions was found to be as large as 18 percent at 210 km at 1700 hours local time in 1962. If substantial amounts of O_2^+ and NO^+ exist above 200 km, then we should expect to find that estimates of the exospheric temperature T_{ex} made by measuring the ion temperature at 230, 260, and 290 km, respectively, would differ markedly, or alternatively, that those estimates of T_{ex} which include observations at 260 or 290 km would yield values closer to the satellite values listed in Table VI than those that depend only on observations at 230 km. Neither of these expectations is borne out, yet the fact that the satellite values of T_{ex} are, on the average, 5 percent higher than the radar values may be indicative of the presence of a small number (5 percent) of O_2^+ and NO^+ ions at 230-km altitude.

There are a number of possible alternative schemes by which the data could be analyzed which might overcome this difficulty. One would be to accept the satellite values of T_{ex} instead of the radar ones. This, however, immediately imposes a difficulty: some of the satellite values are smaller than the corresponding radar ones, and this would require the presence of a lighter ion than O^+ to match the spectral width of the signals. In short, a selfconsistent picture could no longer be obtained if this were done.

A second possible source of error is the assumption of an ion temperature profile [Eq. (8)]. This has been taken from the 1965 CIRA model atmosphere and is therefore ultimately based

upon an integration of the time-dependent heat conduction equation for an atmosphere that always remains in hydrostatic equilibrium, performed by Harris and Priester.[41] This model assumes invariant boundary conditions at an altitude of 120 km and a vertical velocity that is dependent upon atmospheric heating. In this simplified way the dynamical behavior of the atmosphere is included, yet the model does not allow for horizontal motions that must be generated by the heating during the day. Attempts have been made to compute the magnitude of the winds set up,[42-44] but thus far no solution to the problem has appeared, in which motion in three dimensions is permitted, which yields the temperature profile over this altitude range. Volland[44] finds, however, a significant difference between the temperature profile for a one-dimensional solution (Harris-Priester model) and a two-dimensional solution (an E-W section around the equator). The limitations of existing neutral temperature models are discussed further elsewhere.[45]

B. E-Region Temperature

The electron temperature is known to be underestimated by the analysis procedure adopted, since the theoretical spectra were computed for a plasma frequency $f_N = 10$ MHz, whereas the actual plasma density at the heights examined lay in the range from 2.5 to 5.0 MHz. Moorcroft[6] has shown that this type of error leads to an estimate of the electron temperature T'_e that is related to the true value T_e via Eq. (3). Since T_e and N increase with altitude, the Debye length D $[= kt_e/4\pi N_e^2]^{1/2}$ has a value (~ 0.6 cm) that is largely independent of height in the altitude range under study. It follows that $\alpha (= \lambda/4\pi D)$ has a value of the order of 3 to 4 and that the true electron temperatures are approximately 10 percent higher than the values given in Figs. 26(a-e). This correction factor has been applied to the 68-cm results, where at the highest altitudes it may indeed be larger.

C. E-Region Thermal Equilibrium

The conclusion that below about 130 km the E-region is in thermal equilibrium rests upon extrapolating the value of T_e/T_i derived from the lowest spectrum, and is in no way altered by the considerations of Secs. XII-A and XII-B. In this measurement the pulse occupies a height interval of roughly 122 to 152 km. The effect of neutral collisions, evident in the next lower measurement, has been observed by the French group only up to an altitude of 110 km. We expect that by 122 km (i.e., one scale height higher) the effect of collisions should be quite negligible.[36]

D. Seasonal Variation in Composition

Many authors have suggested that the height at which turbulent mixing of the neutral atmospheric constituents ceases to be effective (i.e., the height of the turbopause) may change with season and/or the sunspot cycle. For example, Wright[46] and King[47] have proposed that increased numbers of neutral N_2 molecules at F-region heights are brought about in this or some other way during local summer and are responsible for the seasonal anomaly in F_2 ionization (Sec. VI).

The presence of additional N_2 molecules at F-region heights will cause a larger fraction of the solar EUV to be used in generating N_2^+ ions, which rapidly recombine and do not contribute significantly to the total ion content. In addition, they will increase the rate of loss of O^+ ions via the charge exchange reaction [Eqs. (6) and (7)], which is thought to be the principal loss

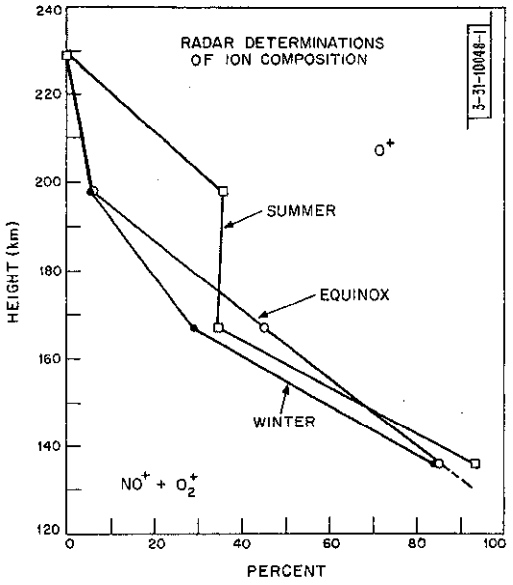

Fig. 28. Results shown in Fig. 27 have here been replotted when averaged over three seasons. There is a tendency during summer for O_2^+ and NO^+ to persist to higher altitudes. This may reflect seasonal changes in neutral composition, which are in turn linked to seasonal anomaly in electron concentration [Fig. 13(c)].

mechanism in the F-region. Since at this latitude the height of the peak of the F_2 region shows little seasonal variation at sunspot minimum,[18] it follows that we should expect a greater abundance of NO^+ ions at altitudes just below the F_2 peak (~230 km), if the explanation is correct. Accordingly, we have averaged the results shown in Fig. 27 into three seasons and replotted them in Fig. 28. On the basis of this figure, it does appear that NO^+ and O_2^+ ions persist to greater altitudes during summer than during winter or equinox, lending some support for this theory. We caution, however, that Fig. 28 is based upon an extremely limited sample of data.

XIII. SUMMARY

A. Daytime Electron Densities

The midday values of $N_{max}F2$ are about twice as large in winter as in midsummer at north temperate latitudes at sunspot minimum. This variation is not reflected in the densities above about 400 km. At these altitudes the density is a maximum at the equinoxes. As a result, the total electron content observed, for example, by Faraday rotation measurements is a maximum at the equinoxes, with the summer minimum being deeper than the winter one. The "thickness" of the F-region (measured by almost any criterion) is a maximum in summer and minimum in winter.

The pattern of behavior seems unrelated to seasonal variations of the electron, ion or neutral temperatures.[27] We are forced to suppose that the seasonal anomaly is the result of increased loss rates in summer,[48] in agreement with many other workers.[46,47] Some support for this conclusion is provided by composition determinations at low altitudes using the 23-cm radar. These results (Fig. 27) are in fair agreement with rocket determinations (Fig. 20), but may overestimate the O^+ abundance at all heights if, in fact, there is a small percentage of NO^+ and O_2^+ ions present at 230 km as suggested by the difference in the satellite and radar determinations of exospheric temperatures. At altitudes above about 170 km, the results suggest a seasonal variation in the relative abundance of O^+ (minimum in summer) that may be related to changes in the neutral composition at these altitudes. However, this conclusion rests upon a small sample of data and should be treated with caution.

In all seasons, h_{max} is a minimum (~200 km) 2 to 3 hours after ground sunrise and subsequently rises to reach a maximum (~290 km) near midnight. About half of this rise (i.e., one scale height of the ionizable constituent) is accomplished during the daytime.

B. Nighttime Electron Densities

In summer and equinoctial months the electron density decreases throughout the night. A number of authors have attempted to derive ionospheric loss rates, e.g., from the observed decay of the layer at night[49] or from eclipse results.[50] These have often yielded conflicting results which, in turn, disagree with laboratory values.[51] The latter are usually much higher than values deduced from the behavior of the F-region and this has given rise to a considerable literature on the question of the maintenance of the nighttime F-layer.[52-55] It appears that at sunspot minimum, the cooling of the protonosphere during the night and the subsequent redistribution of the ionization in the tube of force required to maintain hydrostatic equilibrium can supply a flux of electrons large enough to reduce the apparent loss rates by a considerable factor. In winter the supply of electrons appears to equal or even exceed the loss so that the density either remains constant or increases for a considerable period of the night. It should be noted that the problem of the cooling of a tube of force that was investigated by Geisler and Bowhill[15] has been solved rigorously by Gliddon[16] on the assumption that the electron densities at all altitudes do not change. In actuality, the lowering of the temperature will cause electrons to diffuse to lower altitudes and this, in turn, will serve to convect heat downward. Thus, the problem of the cooling of the protonosphere and the redistribution of the ionization that this produces is a complicated one which still awaits a rigorous solution.

C. Daytime Electron Temperatures

Using the exponential temperature law employed in the 1965 CIRA atmosphere, we have analyzed 23-cm radar measurements made on eight days in 1964. We infer that at E-region heights (below 130 km) thermal equilibrium between electrons and ions prevails, but that above this altitude $T_e > T_i$. The 68-cm measurements show that this inequality persists, at least up to 800 km. In addition, T_i becomes greater than the neutral exospheric temperature above about 300 km. There is little seasonal variation (at least at sunspot minimum) in the temperature profiles obtained.

The daytime electron temperatures show a less rapid rise with altitude up to 300 km than has been predicted, and above this altitude a temperature gradient in T_e persists at all altitudes, i.e., in a region that should be isothermal according to theory. Elsewhere we have suggested[56] that theory and observation can largely be reconciled if there is a deposition of heat above 500 km of the order of 6×10^9 eV/cm^2/sec in winter. This might be produced by a flux of photoelectrons through the 500-km level of $\sim 5 \times 10^8$/cm^2/sec (in winter), which deposit 1.75×10^9 eV/cm^2/sec below 1000 km and 4.25 eV/cm^2/sec in the protonosphere. A. Dalgarno and T. P. Degges (private communication) have postulated that existing theory may be seriously in error by neglecting an important cooling process for the electrons, namely, the reaction

$$e + O(^3P_J) \rightarrow e + O(^3P_{J'}) \qquad (9)$$

If this is so, the cooling rates at low altitudes (where oxygen is abundant) will be higher than supposed. This would probably change the amount of heat transferred locally from the

electrons to the neutrals but will probably not significantly change the conclusion (above) concerning the need for an exospheric heat source.

Local ionospheric heating appears to commence at a solar zenith distance of $\chi = 102 \pm 3°$. The temperature rise at dawn is especially rapid, and results in an expansion of the F-layer which, in turn, lowers the heat loss rates. The reverse happens at sunset, and causes a rapid redistribution of the electrons above the F-layer peak.

D. Nighttime Electron Temperature

While there are no major seasonal changes in the mean daytime values of T_e and T_i, the nighttime values exhibit a dramatic variation, being least in summer and greatest in winter. This is attributed to heat supplied from the protonosphere which continues to be warmed by the conjugate ionosphere throughout the winter night, and supplies heat by conduction. In summer during the period from 2100 to 0300 hours, the heat flux is an order of magnitude smaller and is maintained only by the large reservoir of heat stored in the protonosphere which takes several hours to dissipate. Because the thermal conductivity varies at $T_e^{5/2}$, the heat flux is quite large immediately after sunset, but as T_e falls at the foot of the field line the heat supply is "choked-off" to a much smaller and less rapidly varying value.[15,16]

ACKNOWLEDGMENT

The author would like to acknowledge many members of the staff of the Millstone Hill Radar Observatory for maintaining and operating the ionospheric radar, and in particular, W. A. Reid and J. H. McNally. J. H. MacLeod, J. Upham and Miss D. Tourigny were responsible for the largest part of the data reduction, and Mrs. V. Mason and W. Mason kindly provided the computed signal spectra from which electron and ion temperatures could be obtained by comparison with observed ones. Dr. L. G. Jacchia kindly supplied the values of exospheric temperature obtained by satellite orbital decay observations (Table VI). The author is also grateful to the encouragement of P. B. Sebring and the late V. C. Pineo, and to S. A. Bowhill for many stimulating discussions.

REFERENCES

1. J. V. Evans, "Studies of the F-Region by the Incoherent Backscatter Method," Technical Report 274, Lincoln Laboratory, M.I.T. (24 July 1962), DDC 292730. See also, J.V. Evans and M. Loewenthal, Planet. Space Sci. 12, 915 (1964).
2. _____, "Ionsopheric Backscatter Observations at Millstone Hill," Technical Report 374, Lincoln Laboratory, M.I.T. (22 January 1965), DDC 616607. See also, J.V. Evans, Planet. Space Sci. 13, 1031 (1965).
3. _____, J. Geophys. Res. 70, 1175 (1965).
4. _____, J. Geophys. Res. 70, 4331 (1965).
5. J.A. Fejer, Can. J. Phys. 38, 1114 (1960).
6. D.R. Moorcroft, J. Geophys. Res. 69, 1436 (1964).
7. _____, ibid., 68, 4870 (1963).
8. S.J. Bauer, J. Atmos. Sci. 19, 276 (1962).
9. _____, Electron Density in the Ionosphere and Exosphere, J. Frihagen, Ed. (North Holland, Amsterdam, 1966), p. 270.
10. P.J. Bowen, R.L.F. Boyd, W.J. Raitt and A.P. Wilmore, Proc. Roy. Soc. A281, 504 (1964).
11. T.M. Watt, J. Geophys. Res. 70, 5849 (1965).
12. R.E. Barrington, J.S. Belrose and G.L. Nelms, J. Geophys. Res. 70, 1647 (1965).
13. G.R. Thomas and F.H. Venables, J. Atmos. Terr. Phys. 29, 621 (1967).
14. F. Mariani, J. Geophys. Res. 69, 556 (1965).
15. J.E. Geisler and S.A. Bowhill, J. Atmos. Terr. Phys. 27, 1119 (1965).
16. J.E.C. Gliddon, Aeronomy Laboratory Report No. 12, University of Illinois, Urbana (1966).
17. K.C. Yeh and B.J. Flaherty, J. Geophys. Res. 71, 4557 (1966).
18. W. Becker, Electron Density Profiles in the Ionosphere and Exosphere, J. Frihagen, Ed. (North Holland, Amsterdam, 1966), p. 218.
19. L. Thomas, J. Geophys. Res. 71, 1357 (1966).
20. H.C. Carlson, Electron Density Profiles in the Ionosphere and Exosphere, J. Frihagen, Ed. (North Holland, Amsterdam, 1966), p. 478.
21. _____, J. Geophys. Res. 71, 195 (1966).
22. _____, CRSR 212, Cornell University, Ithaca, New York (1965).
23. _____, private communication.
24. H. Carru, M. Petit and P. Waldteufel, J. Atmos. Terr. Phys. 29, 351 (1967).
25. A.V. da Rosa, J. Geophys. Res. 71, 4107 (1966).
26. J.E. Geisler and S.A. Bowhill, J. Atmos. Terr. Phys. 27, 457 (1965).
27. L.G. Jacchia, Space Res. 5, 1152 (1965).
28. P. Stubbe, Electron Density Profiles in the Ionosphere and Exosphere, J. Frihagen, Ed. (North Holland, Amsterdam, 1966), p. 249.
29. H.A. Taylor and H.C. Brinton, J. Geophys. Res. 66, 2587 (1961).
30. M. Petit, Ann. Geophys. 19, 63 (1963).
31. P.M. Banks, Ann. Geophys. 22, 577 (1966).
32. _____, Planet. Space Sci. 15, 77 (1966).
33. T. Yonezawa, Space Sci. Rev. 5, 3 (1966).
34. V.G. Istomin, Planet. Space Sci. 9, 179 (1962).
35. J.C. Holmes, C.Y. Johnson and J.M. Young, Space. Res. 5, 756 (1965).
36. J.P. Dougherty and D.T. Farley, J. Geophys. Res. 68, 5473 (1963).
37. N.W. Spencer, L.H. Brace, G.R. Carignan and D. Taeusch, J. Geophys. Res. 70, 2665 (1965).

38. L.H. Brace, Second Conference on Direct Aeronomic Measurements in the Lower Ionosphere – an Informal Conference Record, Aeronomy Report No. 10, Ed. by C.F. Sechrist, Jr. and J.S. Shirke (University of Illinois, Urbana, 1966).

39. W.B. Hanson, Space Res. 3, 282 (1963).

40. W.C. Knudsen, J. Geophys. Res. 71, 4669 (1966).

41. I. Harris and W. Priester, Technical Note D-1444, NASA (1962).

42. J.E. Geisler, J. Atmos. Terr. Phys. 28, 703 (1966).

43. H. Kohl and J.W. King, J. Atmos. Terr. Phys. 29, 1045 (1967).

44. H. Volland, Space Res. 7, 1193 (1967).

45. J.V. Evans, Solar Terrestrial Physics, Ed. by W.S. Newman and J.W. King (Academic Press, London, 1967), Chap. 9.

46. J.W. Wright, J. Geophys. Res. 68, 4379 (1963).

47. G.A.M. King, Planet. Space Sci. 9, 95 (1962).

48. H. Rishbeth and C.S.G.K. Setty, J. Atmos. Terr. Phys. 20, 263 (1961).

49. J.S. Nisbet and D. McCory, Electron Density Profiles in the Ionosphere and Exosphere, J. Frihagen, Ed. (North Holland, Amsterdam, 1965), p. 530.

50. T.E. Van Zandt, R.B. Norton and G.N. Stomehocker, J. Geophys. Res. 65, 2003 (1960).

51. P.M.C. Dickenson and J. Sayers, Proc. Phys. Soc. 76, 157 (1960).

52. T. Yonezawa, J. Res. Lab. Japan 12, 65 (1965).

53. _____, Space Res. 49 (1965).

54. W.B. Hanson and T.N.L. Patterson, Planet. Space Sci. 11, 1035 (1963).

55. J.E. Geisler, J. Geophys. Res. 72, 81 (1967).

56. J.V. Evans, Planet. Space Sci. 15, 1557 (1967).

DOCUMENT CONTROL DATA – R&D

(Security classification of title, body of abstract and indexing annotation must be entered when the overall report is classified)

1. ORIGINATING ACTIVITY *(Corporate author)* Lincoln Laboratory, M.I.T.	2a. REPORT SECURITY CLASSIFICATION Unclassified 2b. GROUP None

3. REPORT TITLE

Millstone Hill Thomson Scatter Results for 1964

4. DESCRIPTIVE NOTES *(Type of report and inclusive dates)*

Technical Report 430

5. AUTHOR(S) *(Last name, first name, initial)*

Evans, John V.

6. REPORT DATE	7a. TOTAL NO. OF PAGES	7b. NO. OF REFS
15 November 1967	52	56

8a. CONTRACT OR GRANT NO. AF 19(628)-5167 b. PROJECT NO. 649L c. d.	9a. ORIGINATOR'S REPORT NUMBER(S) Technical Report 430 9b. OTHER REPORT NO(S) *(Any other numbers that may be assigned this report)* ESD-TR-67-563

10. AVAILABILITY/LIMITATION NOTICES

This document has been approved for public release and sale; its distribution is unlimited.

11. SUPPLEMENTARY NOTES	12. SPONSORING MILITARY ACTIVITY
None	Air Force Systems Command, USAF

13. ABSTRACT

Thomson scatter (incoherent backscatter) observations of the ionosphere were made at Millstone Hill at a wavelength of 68 cm during 1964, for 30-hour periods every two weeks. These data have been employed to derive the mean hourly F-region (200 to 700 km) electron density profile and electron and ion temperature curves in each month. The results are presented in this report, together with the derived seasonal variation of electron density (at 0600, 1200, 1800 and 2400 hours local time) and the average daytime (0900 to 1500) and nighttime (2100 to 0300) electron and ion temperature behavior.

Separate measurements with a 23-cm radar permitted the temperature results reported to be extended to lower altitudes (~130 km) and, in addition, provided information concerning the ionic constituents between 130 and 230 km.

Although 1964 was at sunspot minimum, the seasonal variation in f_0F2 was quite evident. It is shown that this feature is strictly associated with the peak of the layer and that densities above 400-km altitude are highest at the equinoxes. No seasonal variations of temperature are found which might be large enough to account for the phenomenon. At night the peak densities are highest in summer, and the temperatures at all altitudes highest in winter. This last effect is believed largely due to heat conducted from the protonosphere, which in winter continues to be heated by photoelectron escape from the conjugate ionosphere which remains sunlit throughout the night.

14. KEY WORDS

Millstone radar
scattering